

*When you can't make them see the light, make them feel the heat.*

Ronald Regan

# 3

## Optical Imaging

### 3.1 AUTHORS

Sabrina Brigadoi and Robert J. Cooper

### 3.2 INTRODUCTION

Many biological tissues, including human scalp and skull, are relatively transparent to light in the near-infrared range. The oxygenated and de-oxygenated forms of haemoglobin (the molecule that carries oxygen around the bloodstream) happen to exhibit distinct absorption spectra in this wavelength range. Optical methods can exploit these properties of near-infrared light to measure cerebral activity. Optical techniques are portable and completely non-invasive and can therefore be applied to almost any population, including children and infants.

This chapter provides an overview of optical methods, their advan-

## Optical Imaging

---

tages, disadvantages and applications. The chapter is organized as follows: in section 3.3, a brief history of the origins and development of optical methods is presented. Section 3.4 describes the theory behind optical techniques and the process of image reconstruction. The concept of the functional haemodynamic response is introduced and explained in the context of optical techniques. In the same section, strengths and weaknesses of optical methods are discussed. Section 3.5 describes a number of key factors that must be considered when applying optical techniques including how to configure a measurement array. Section 3.5 also provides an overview of typical signal processing and statistical analysis methods and lists the open source software tools available for optical signal processing. Finally, in section 3.6, examples of the application of optical methods, in three different contexts, are provided.

### 3.3 HISTORICAL NOTES

Optical methods have been used since the first decades of the 20th century to investigate tissue. In the 1940s, Glenn Millikan pioneered the method of tissue spectrophotometry: demonstrating the ability to measure haemoglobin and myoglobin deoxygenation in cat muscle, and building the first muscle oximeter [Millikan, 1937]. At the same time, Matthes and Gross [1939] discovered that light in the red to near-infrared range was sensitive to both oxyhaemoglobin and deoxyhaemoglobin concentrations ( $\text{HbO}$  and  $\text{HbR}$  respectively). Further development of these concepts led Takuo Aoyagi to develop the first pulse oximeter in 1972, which was able to measure arterial saturation by taking advantage of pulsatile blood volume variations. In 1975, the pulse oximeter was used in patients for the first time and has since become an essential clinical monitoring device [Severinghaus and Honda, 1987].

In 1977, Frans Jöbsis, who is considered the father of in vivo near-infrared spectroscopy (NIRS), performed the first 'transcranial spectroscopy' experiment, demonstrating that light in the red and near-infrared range can travel through the scalp, skull, cerebrospinal fluid, into the

### 3.3 Historical notes

---

brain tissue and return to be measured at the surface [Jöbsis, 1977]. For the first time, optical methods were shown to be able to detect brain oxygenation changes in adults.

In the 1980s, near-infrared spectroscopy was applied to measure tissue oxygen saturation in newborn infants and adults in the clinical environment [Brazy et al., 1985, Ferrari et al., 1985]. In the following year, developments in optical electronics, pioneered by David Delpy, led to the first quantitative measure of haemoglobin changes in sick infants [Wyatt et al., 1986]. The system designed by Delpy [Cope and Delpy, 1988] resulted in the first commercial NIRS system, the NIRO-1000, built by Hamamatsu Photonics K.K. in 1989 [Ferrari and Quaresima, 2012].

In 1992, the simultaneous publication of three papers [Bandettini et al., 1992, Kwong et al., 1992, Ogawa et al., 1992] gave birth to functional magnetic resonance imaging (fMRI). It was demonstrated that the intensity of an image acquired with MRI was dependent on the amount of deoxy-haemoglobin present in the tissues, which led directly to the measurement of the Blood Oxygen Level Dependent (BOLD) signal (see chapter??). The field of fMRI developed extremely quickly, becoming the predominant imaging technique in neuroscience.

Functional near-infrared spectroscopy (fNIRS), the application of near-infrared spectroscopy to study brain function, was demonstrated in the same era. The first fNIRS experiments were carried out in adults in 1991 and 1992 by research groups in three different countries: in Japan, by Hoshi and Tamura [1993] and Kato et al. [1993], in Germany by Villringer et al. [1993] and in the US by Chance et al. [1993]. These studies showed characteristic increases in HbO and decreases in HbR following visual stimulation or cognitive tasks using single location measurements [Ferrari and Quaresima, 2012]. In 1994, the first clinical fNIRS study was performed on schizophrenic patients [Okada et al., 1994], while in 1998 Meek et al. [1998] measured the first functional brain response in awake infants using fNIRS and a visual stimulus.

The next step in the development of fNIRS technology was moving from single-location measurements to multi-channel approaches. The

## Optical Imaging

---

first multi-channel fNIRS system was developed by Hitachi in 1994 [Watanabe et al., 1994], and was used in 1995 by Maki et al. [1995], who was the first to use fNIRS data to produce images. By measuring the fNIRS signal from 10 different locations, Maki et al. [1995] were able to create two-dimensional maps of haemoglobin concentration changes and, with the help of MRI images, to associate these changes with a specific area of the cerebral cortex.

In the following years, advances in the mathematical and computational modelling of light propagation in highly scattering biological tissues lead to the birth of diffuse optical tomography (DOT) [Boas et al., 2001, Hebdon and Delpy, 1997]. In DOT, three-dimensional images of brain oxygenation can be recovered by solving an ill-posed, non-linear inverse problem [Arridge, 1999]. In 2001, the first whole-head 3D tomographic images of the adult brain showed the distribution of haemoglobin concentration changes during a Valsalva manoeuvre [Bluestone et al., 2001]. One year later, the first 3D images of the neonatal brain were reconstructed, showing a cerebral haemorrhage in a pre-term infant [Hebdon et al., 2002]. With continuous developments in both hardware and software, it was possible to produce systems with many more channels and perform 'high-density' DOT. This was first demonstrated by Zeff et al. [2007], who presented retinotopic maps of the adult visual cortex, with a spatial resolution comparable to fMRI. Recently, Eggebrecht et al. [2014] presented a high-density DOT system that has sufficient sampling density and scalp coverage to map higher order, distributed brain function.

The volume of optical imaging research has increased exponentially in recent years, a fact celebrated by the publication of a special issue of Neuroimage that marked twenty years of fNIRS research. Optical methods have become an established neuroimaging tool particularly in applications that are unsuitable for fMRI (see chapter ??) or Positron Emission Tomography (PET) (see chapter ??) [Boas et al., 2014].

For a more detailed history of functional near-infrared spectroscopy, see [Ferrari and Quaresima, 2012].

### **3.4 PHYSICAL PRINCIPLES**

#### **3.4.1 NIRS THEORY**

Optical imaging of the in-vivo human brain is possible because of the way different wavelengths of light interact with biological tissues. Light interacts with tissue via two fundamental mechanisms: absorption, where the energy of a photon is transferred to the medium and scattering, where the path of the photon is altered but its energy remains (in almost all cases) unchanged. The likelihood of these interactions occurring within a given medium are determined by the absorption and scattering coefficients of that medium, which are both dependent on the wavelength of light.

Light in the lower visible range (i.e. blue and green) is heavily absorbed by melanin in the skin and by the oxygenated and deoxygenated forms of haemoglobin in the blood. However, the absorption coefficients of melanin and haemoglobins decrease by several orders of magnitude between the wavelengths of 600 and 700 nm. As a result, red and near-infrared light (with wavelengths above  $\sim$ 650 nm) can be successfully transmitted through several centimetres of tissue. This is a phenomenon that is easily observed in everyday life: when you cover a white light with your hand, the light you see is red, simply because the other colours of visible light are absorbed by your tissues (Fig. 3.4.1a). For longer near-infrared wavelengths (above 900 nanometres), water becomes very strongly absorbing. Between 650 and 900 nm, there therefore exists an 'optical window' (Fig. 3.4.1b), through which we can use light to study human tissues, including the brain.

Near-infrared light does not travel through tissue in a straight line, unlike (for example) x-ray radiation. Of the two fundamental interactions between light and matter, it is scattering that dominates the propagation of near-infrared light through biological tissues. The scattering coefficient for near-infrared light in skin is typically 100 times greater than the absorption coefficient, meaning that a photon is 100 times more likely to be

## Optical Imaging

---

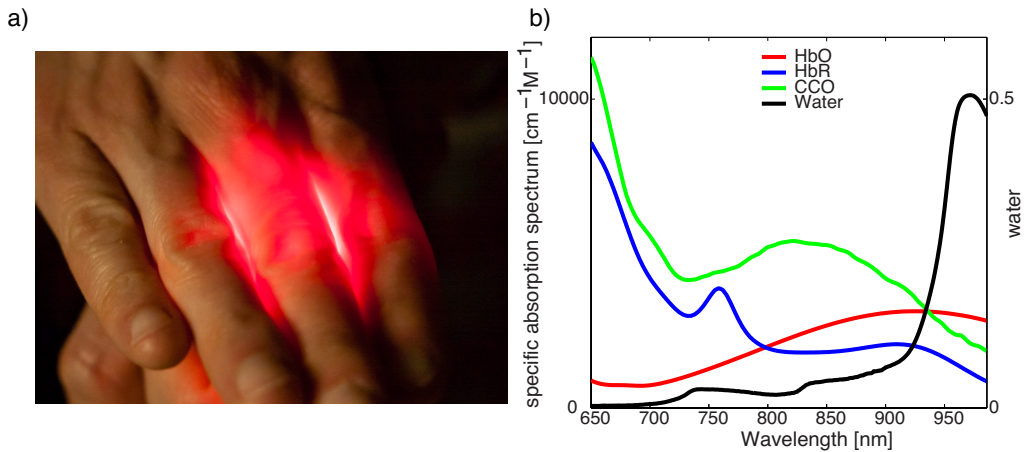


**Figure 3.4.1: Near-infrared light properties.** a) Demonstration of the transparency of human tissues to red light: covering a white light with a hand, all colours of visible light but red are absorbed by the human tissues. b) Specific absorption spectra of oxy- (HbO) (in red), deoxy-haemoglobin (HbR) (in blue) and cytochrome oxidase (CCO) (in green) and absorption spectrum of water (in black). Between 650 and 900 nm there is an 'optical window', through which we can use light to study human tissues.

scattered than absorbed, per unit distance travelled. As a result, the path of a near-infrared photon in tissue resembles a random walk. The light field produced by placing a near-infrared source in contact with tissue is therefore highly diffuse.

NIRS is the oldest method of exploiting the optical window to study the human brain in-vivo. In its simplest form, NIRS requires near-infrared light to be directed into the scalp at one location (usually via an optical fibre) and detected at a second location (also usually via an optical fibre). A source and detector together form one 'channel'. Light from the source fibre will travel diffusely through the underlying tissues and a small proportion will be scattered back to the detector fibre at the surface. Fig. 3.4.2a shows a fluence distribution in an adult head for a single source position on the scalp. This model illustrates where near-infrared light injected at the source location will travel. Note how the fluence decreases rapidly with depth. Fig. 3.4.2b shows a classic 'photon measurement density function' (or PMDF). This distribution can be thought

of as giving the probability that a detected photon will travel through a given region of tissue. The greater this probability, the more sensitive the NIRS measurement will be to changes in the optical properties of that region. It should be clear from this distribution that the NIRS measurement is highly sensitive to changes occurring directly beneath the source and detector locations.

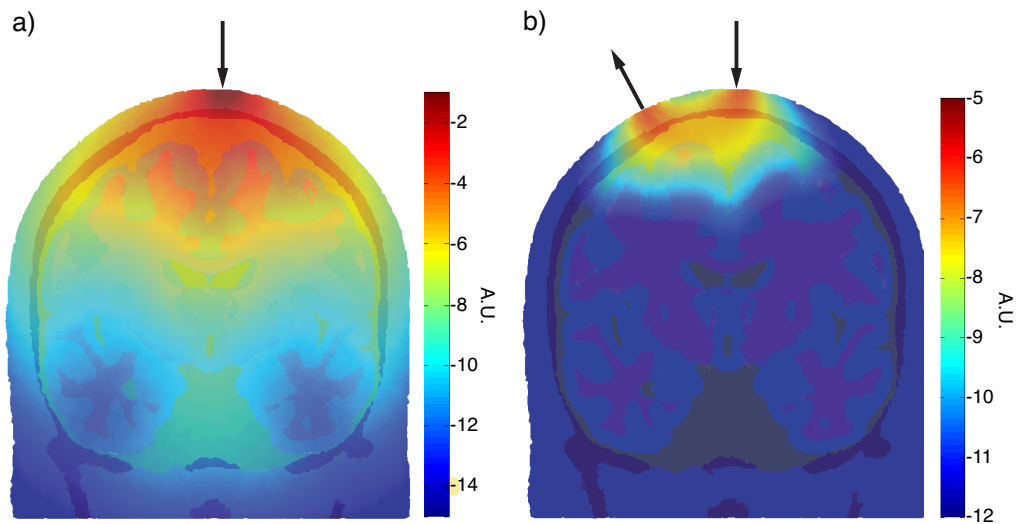


**Figure 3.4.2: Fluence and PMDF.** a) Example of fluence distribution in an adult head for a single source position on the scalp. The log of the sensitivity is displayed for visualization purposes. b) Example of photon measurement density function (PMDF), which can be thought of as a probability distribution for a photon leaving the source and being collected at the detector position to travel through a given region of tissue.

The separation between the source and detector locations will affect what proportion of the detected photons will have travelled through brain tissue; the greater the separation, the greater the proportional sensitivity to the brain. However, as is clear from Fig. 3.4.2a, the measured optical intensity will decrease exponentially with source-detector separation. The optimal separation between a NIRS source and detector is therefore a balance between maximising the proportional sensitivity to brain tissue while still detecting enough light to allow reliable measurements.

The simplest NIRS systems, referred to as 'continuous wave' (CW) systems measure only the intensity of the light incident at the detector. In

## Optical Imaging

---

order to relate measurements of intensity to measurements of physiologically relevant parameters, CW-NIRS processing will often invoke the modified Beer-Lambert law (MBLL):

$$\frac{I}{I_0} = \exp^{-xD\mu_a} + \text{Losses} \quad (3.1)$$

where  $I_0$  and  $I$  are the input and output intensities respectively,  $x$  is the separation between source and detector and  $\mu_a$  is the absorption coefficient of the medium. The variable  $D$  is known as the differential path-length factor (or DPF). The DPF is included to account for the fact that in a scattering medium, photons travelling between the source and detector will not travel in a straight line. The product  $xD$  represents the average distance photons will travel through the tissue to reach the detector. For a non-zero scattering coefficient, the DPF will always be greater than 1. The *Losses* factor accounts for the photons that, because of the geometry of the problem, are not observed by the detector.

In equation 3.1, the *Losses* factor, the input intensity  $I_0$  and the absorption coefficient  $\mu_a$  are all unknown, while the output intensity  $I$  and source-detector separation  $x$  are measured and the DPF ( $D$ ) can be estimated. The absorption coefficient,  $\mu_a$ , is what we wish to determine, but direct calculation of  $\mu_a$  is impossible in this context because of the number of unknowns. Instead, CW-NIRS systems are used to measure changes in intensity between two points in time, such that:

$$\ln \frac{I_2}{I_0} - \ln \frac{I_1}{I_0} = \ln \frac{I_2}{I_1} = xD\Delta\mu_a \quad (3.2)$$

where  $I_1$  and  $I_2$  are the measured intensities at two distinct points in time and  $\Delta\mu_a$  is the change in absorption coefficient. This approach assumes that the *Losses*, the input intensity  $I_0$  and the DPF ( $D$ ) do not change between the two time points. This assumption is generally reasonable over the course of an experiment.

A change in the absorption coefficient of tissue at a given wavelength

### 3.4 Physical principles

---

$(\Delta\mu_{a|\lambda})$  is linearly related to the changes in concentration of absorbing molecules in that tissue via:

$$\Delta\mu_{a|\lambda} = \epsilon_{HbO|\lambda}\Delta C_{HbO} + \epsilon_{HbR|\lambda}\Delta C_{HbR} + \dots \quad (3.3)$$

where  $\epsilon_{HbO|\lambda}$  and  $\epsilon_{HbR|\lambda}$  are the specific extinction coefficients of oxyhaemoglobin (HbO) and deoxyhaemoglobin (HbR) at wavelength  $\lambda$  and  $\Delta C_{HbO}$  and  $\Delta C_{HbR}$  are the changes in concentration of HbO and HbR in the measured volume of tissue. Although tissue contains many more absorbing molecules (including melanin, water, lipids and cytochrome oxidase (CCO)), these absorbers are typically neglected either because of their negligible concentration or because they are assumed to remain constant for the duration of the experiment.

In order to measure the change in concentration of both oxyhaemoglobin and deoxyhaemoglobin, it is necessary to measure  $\Delta\mu_{a|\lambda}$  at more than one wavelength. NIRS systems typically operate at two wavelengths, usually with one above and one below the point at which HbO and HbR demonstrate the same absorption coefficient (known as the isosbestic, at 808 nm, Fig. 3.4.1b). These two wavelengths of light must be directed into tissue at the same location to obtain an accurate NIRS measurement. In most NIRS systems therefore, the source optical fibre is in fact a bundle of optical fibres that is divided in two at the system end, with each half coupled to a source of a different wavelength.

There are a number of bespoke and commercial NIRS systems that use multiple wavelengths, or even broadband sources. Recording at 3 or more wavelengths can be used to simply improve the reliability of measurements of  $\Delta C_{HbO}$  and  $\Delta C_{HbR}$  or can be used to resolve additional chromophores; measuring at  $N$  wavelengths theoretically allows the recovery of the change in concentration of  $N$  chromophores, and there is increasing evidence that measuring the concentration changes of cytochrome oxidase in addition to  $\Delta C_{HbO}$  and  $\Delta C_{HbR}$  provides additional physiological information than is provided by  $\Delta C_{HbO}$  and  $\Delta C_{HbR}$  alone.

## Optical Imaging

---

Continuous-wave NIRS has a number of limitations. The most fundamental is that CW-NIRS cannot be used to obtain absolute measures of chromophore concentration and instead is used to measure changes. A secondary limitation is that the *Losses* and DPF ( $D$ ) parameters of equation 3.2 are dependent on the scattering coefficient of the medium. As a result, any change in the scattering coefficient of the sampled tissue will be misinterpreted as a change in absorption coefficient; CW-NIRS cannot separate the effects of absorption and scatter. In addition, because the DPF parameter must be estimated, it constitutes a source of inaccuracy in the scaling of CW-NIRS measurements. The use of the DPF inherently requires the assumption that the mean pathlength travelled by the detected photons is linearly dependent on the source-detector separation and independent of everything else. In fact, the mean pathlength (and therefore DPF) is location and subject specific, and has an asymptotic relationship with source-detector distance. Using the same DPF value for a large range of source-detector separations will therefore introduce relative scaling errors between those channels. Lastly, CW-NIRS is subject to partial-volume errors: if a change in chromophore concentration only occurs in a small proportion of the volume sampled by the CW-NIRS channel (as is always the case for functional studies) the measured change in chromophore concentration will be underestimated by a factor equal to the ratio of the activated volume to the sampled volume.

There are a number of hardware and signal processing advances that have successfully minimized the impact of many of the limitations of continuous-wave NIRS. The simplest is use of spatially-resolved spectroscopy (SRS). By using multiple detectors spaced a few millimetres apart, SRS-NIRS takes advantage of the approximately linear decrease in the logarithm of measured intensity as a function of distance from the source [Suzuki et al., 1999]. In this manner, SRS-NIRS systems are able to obtain an absolute measurement of the ratio of oxyhaemoglobin to the sum of oxyhaemoglobin and deoxyhaemoglobin, which is referred to as 'tissue oxygen saturation'. Although this approach depends on a number of assumptions, and is sensitive to variation in the optical coupling

### **3.4 Physical principles**

---

between detectors, single or dual-channel SRS-NIRS systems are popular, commercially available and increasingly used for clinical assessment [Pellicer et al., 2013].

A more sophisticated approach is to use a NIRS system that can measure more than just optical intensity. Frequency-domain (FD-NIRS) systems use detectors with high temporal resolution and sources that are modulated at  $\sim 100$  MHz to provide measures of both optical intensity and phase. The phase difference between the input and detected light can be used to calculate the mean pathlength, removing the need to estimate the DPF. Time-domain (TD-NIRS) systems go one step further: using pulsed laser sources and sensitive photon-counting detectors, TD-NIRS systems measure the time-of-flight of individual photons. By sampling over multiple pulses, TD-NIRS systems output histograms of photon flight times. Each histogram (referred to as a Temporal Point Spread Function (TPSF)) contains significantly more information than either a CW-NIRS or FD-NIRS measurement. Both FD-NIRS and TD-NIRS systems can, under certain circumstances, be used to obtain absolute measures of tissue chromophore concentration.

#### **3.4.2 HAEMODYNAMIC RESPONSE**

While NIRS methods can be used to measure spontaneous fluctuations in chromophore concentrations, the most common application of NIRS approaches is in the study of functional activation. The typical functional NIRS (fNIRS) experimental paradigm involves inducing a change in the cortical concentration of oxyhaemoglobin and deoxyhaemoglobin by repeated application of an external stimulus. Neurons in the areas of the cerebral cortex associated with the processing of that stimulus will exhibit increased electrochemical activity and with it an increased demand for both oxygen and glucose. The brain possesses an intricate and targeted mechanism for the maintenance of neuronal oxygen and glucose levels that is broadly referred to as 'neurovascular coupling'. While the exact processes of neurovascular coupling are still the subject of active

## Optical Imaging

---

research, increased neuronal activation leads to a release of vasoactive chemicals that promote localized vasodilation and a localized increase in cerebral blood flow. While naively one might expect that an increase in neuronal activity would manifest as a localized decrease in cerebral oxygenation, the functional response of the cerebral vasculature ensures that the opposite is in fact true. The increase in oxygen delivery via functional hyperaemia is significantly larger than the increase in oxygen demand due to neuronal activity. The ground-breaking positron emission tomography study by [Fox and Raichle \[1986\]](#) allowed this 'flow-demand ratio' to be calculated for the first time, and a range of studies (using various methodologies) have placed this ratio at between 2 and 10 in the healthy human brain [[Mintun et al., 2001](#)].

Because of the overcompensation in cerebral blood flow, the impact of functional stimuli on fNIRS-measured parameters will typically consist of a localized increase in oxyhaemoglobin concentration and concomitant decrease in deoxyhaemoglobin concentration, as oxygenated blood floods into the active brain region. An example of this classic haemodynamic response function (HRF) is shown in Fig. 3.4.3. The amplitude of these responses is typically small. In fact, the HRF is rarely apparent in un-processed fNIRS data because its impact is smaller than that of systemic physiological variations due to, for example, cardiac pulsation, respiration and blood pressure.

It is important to note that the haemodynamic response that is at the heart of functional NIRS methods is exactly the same physiological process that gives rise to the Blood-Oxygen Level Dependent (BOLD) signal of functional Magnetic Resonance Imaging (see chapter ??). The deoxyhaemoglobin molecule is paramagnetic, and the decrease in concentration of deoxyhaemoglobin due to functional hyperaemia is the primary source of a positive BOLD signal. The ability of NIRS approaches to differentiate between changes in the oxygenated and deoxygenated forms of haemoglobin has lead a number of researchers to apply fNIRS simultaneously with fMRI in order to investigate the physiological origins of

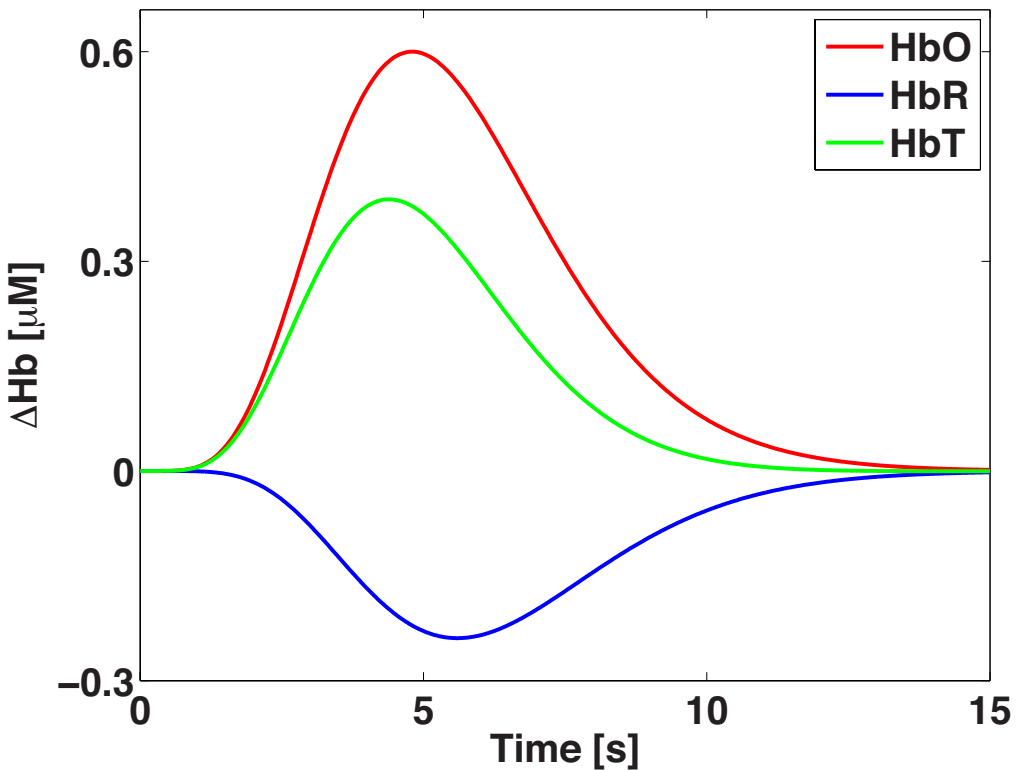


**Figure 3.4.3: Haemodynamic response.** Example of haemodynamic response function (HRF). An increase in HbO (in red) and a decrease in HbR (in blue) are expected after stimulus presentation. In green the total haemoglobin (HbT), given by the sum of HbO and HbR, is displayed.

the BOLD signal [Huppert et al., 2006, Steinbrink et al., 2006].

As NIRS methods are sensitive to the same physiological marker of neuronal activation as fMRI, NIRS methods can also be used to study the oscillations in neuronal activity that occur spontaneously without the application of overt external stimuli. The temporal correlation of these oscillations across distinct brain regions is a manifestation of the brain's functional organisation, and allows the brain to be studied in subjects who are nominally at rest. This 'resting-state' functional connectivity has been widely observed with fMRI and fNIRS approaches in a range of ages and pathologies [Eggebrecht et al., 2014, Ferradal et al., 2015, Sasai et al., 2012, White et al., 2009].

## Optical Imaging

---

### 3.4.3 IMAGE RECONSTRUCTION

Because the interactions between near-infrared light and biological tissue are dominated by scattering, achieving high-resolution imaging using optical methods is challenging. However, all multi-channel NIRS measurements will contain significant spatial information. The use of arrays of NIRS measurements to produce maps of cortical function is referred to by several terms which have rather subtle distinctions. The exact usage of these terms varies throughout the field, but the authors use the terms as follows: 'NIRS' describes methods where single-channel, or multiple sparsely-arranged channels are applied and the data is examined on a channel-by-channel basis (Fig. 3.4.4a). 'Diffuse Optical Topography' uses multiple channels with a fixed source-detector separation to produce two-dimensional maps of cerebral haemodynamics (Fig. 3.4.4b). Lastly, 'Diffuse Optical Tomography' (DOT) uses multiple channels with a range of source-detector separations and overlapping PMDFs to produce three-dimensional maps of cerebral haemodynamics (Fig. 3.4.4c).

The process of producing images from near-infrared measurements is complex, and is an active area of research. In its most general form, the problem of image reconstruction can be stated as:

$$y = A(x) \quad (3.4)$$

where  $y$  denotes the measured data,  $x$  is a representation of the optical properties of the object under investigation as a function of location (i.e.  $x$  is the image) and  $A$  is a forward operator that maps from the image space to the measurement space. Determining the image ( $x$ ) from this equation is an ill-posed and under-determined non-linear inverse problem, which is mathematically and computationally difficult to solve. While these challenges have been overcome in a number of situations [Austin et al., 2006, Enfield et al., 2013], the more common approach to image reconstruction is to attempt (in a manner somewhat analogous to the

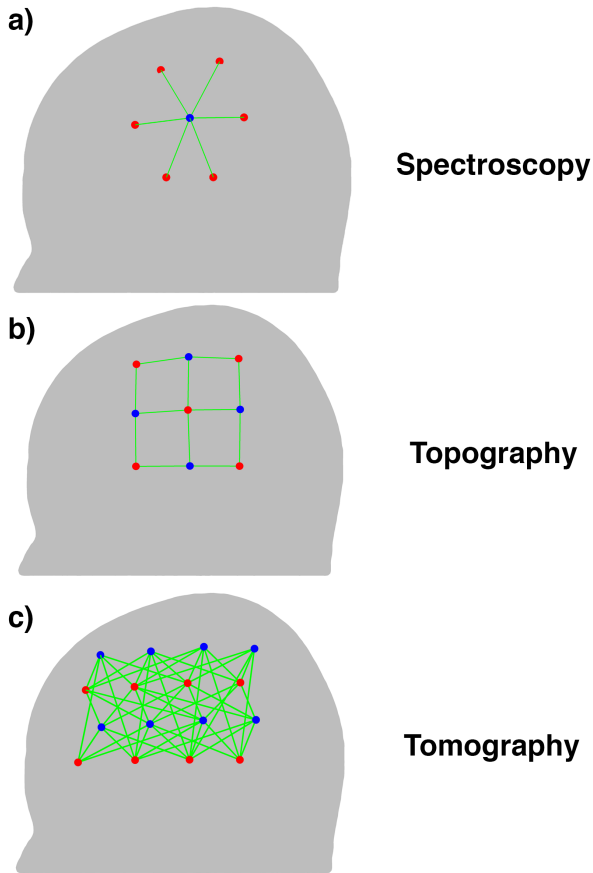


**Figure 3.4.4: NIRS source/detector configurations.** Example of source/detector distribution for a) spectroscopy, b) topography and c) tomography. Sources are visualized in red, detectors in blue and green lines represent the channels.

formation of equation 3.2) to reconstruct images of changes in cerebral haemodynamics. The assumption that these changes are small and have little effect on the path that the detected light has travelled allows us to linearize equation 3.4 such that:

$$\Delta y = J \Delta x \quad (3.5)$$

where  $\Delta y$  is a vector of the changes in the measured optical parameters (such as change in intensity ( $I_2 - I_1$ )),  $\Delta x$  is the change in optical properties in the discretized image space and  $J = dA/dx$  is the Jacobian sensitiv-

## Optical Imaging

---

ity matrix. This linearization approach significantly simplifies the optical image reconstruction problem, and is well suited to the reconstruction of images of small changes in cerebral haemodynamics due to functional stimulation.

In practice, the process of diffuse optical image reconstruction has three distinct phases. The first is to obtain a discretized model of the object under investigation (usually the head and brain), in the form of a finite element mesh or voxelized volume. The second is use this physical representation of the head as a solution space for models of photon transport. These models predict how near-infrared light will travel from each source location on the scalp through the tissues of the head, producing a fluence distribution such as that shown in Fig. 3.4.2a. This allows us to determine how our measurements (of intensity, phase difference etc.) would be altered by a given change in the optical properties within our solution space. This is known as solving the *forward problem*, and yields the Jacobian sensitivity matrix  $J$ . Each row of the matrix  $J$  represents the sensitivity of a given channel, and has the form depicted in Fig. 3.4.2b. The third and final phase of optical image reconstruction is to solve the *inverse problem*, which requires the matrix  $J$  to be inverted. Because we have many more unknowns than measurements (i.e.  $\Delta x$  has many more elements than  $\Delta y$ ), the inversion of  $J$  is not mathematically exact and requires a process of regularization. Our image in the solution space,  $\Delta x$ , can then be determined by taking the matrix multiplication of the inverted Jacobian and the data vector  $\Delta y$ .

The accuracy of diffuse optical image reconstruction is heavily dependent on the accuracy of the chosen discretized head model. The best-practice approach to this problem is to obtain a high-resolution structural MRI image of each subject, and use this image to produce a bespoke, multi-layered finite element mesh or voxelized tissue mask. Each head model can then be segmented into 5 tissue types which possess distinct optical properties: scalp, skull, cerebrospinal fluid, grey matter and white matter. The locations of the near-infrared source and detector can then be registered to the scalp surface of the head model. The *forward problem* can

then be solved within this highly accurate anatomical representation of the subject. This individualized approach requires that each subject undergoing diffuse optical imaging must also undergo an MRI scan. This undermines one of the major advantages of diffuse optical imaging: the technology is portable and can be applied to subjects and patients who may be unsuitable for the typical scanning environment. Several research groups have addressed this problem, and the use of generic MRI atlases has proven effective, but does introduce additional localization errors [Cooper et al., 2012a, Ferradal et al., 2014].

#### 3.4.4 STRENGTHS AND WEAKNESSES

The fundamental physical limitations described above (equations 3.1, 3.2, 3.3) should make it clear why the use of NIRS methods to measure absolute physiological values is extremely challenging. Despite these limitations and the approximations involved, CW-NIRS methods are currently undergoing clinical trials in the monitoring of neonatal cerebral oxygenation [Pellicer et al., 2013], and the technological advances of FD and TD-NIRS will improve the accuracy and utility of these methods in the coming years. From the perspective of functional neuroimaging, diffuse optical tomography is extremely promising but also has a number of weaknesses.

Diffuse optical imaging methods are unlikely to ever truly match the high spatial resolution and localization accuracy that is increasingly being demonstrated by fMRI. This is fundamentally because of the physical limitations of imaging a highly scattering medium and because of the need to spatially register diffuse optical measurements to an anatomical model. Depth resolution is also a significant challenge, with few diffuse optical imaging systems claiming sensitivity deeper than a few centimetres. It is therefore important to clearly state that diffuse optical methods should not be used to map human brain function if fMRI is readily available and suitable for the experimental population and the chosen paradigm. That said, diffuse optical imaging is well suited to the study

## Optical Imaging

---

of infants, children and vulnerable adults. It is silent, allowing for uncorrupted studies of auditory function, and it is relatively robust to motion artifacts. However, the greatest advantage of diffuse optical methods lies in their ability to perform functional brain imaging in an unrestricted environment. In the near future, it is likely that diffuse optical imaging systems will become truly wearable [Piper et al., 2014]. This technological leap will open a whole new branch of neuroscience as it become possible to obtain images of brain function in everyday circumstances and real-world environments.

Historically, the uptake of diffuse optical imaging has been hampered by a number of fundamental challenges. These include the difficulty of producing an instrument and patient interface with a high enough number of channels to achieve a high spatial resolution and good scalp coverage. This remains an issue in commercially available systems and in practice, users have to strike a balance between channel density and coverage. As should be apparent from Fig. 3.4.2b, diffuse optical imaging methods are also highly sensitive to superficial tissues, particularly the scalp, and this can impact specificity. The effects of cardiac pulsation, respiration and systemic and localized changes in blood pressure are all apparent in diffuse optical imaging data. These physiological confounds can span the same frequency distribution as the Haemodynamic Response Function, and can even be temporally correlated with external stimuli. For example, it is extremely common that the heart rate and blood pressure of a subject will increase when they are requested to begin a stimulation task, and these changes can be misinterpreted as a functional change in the brain. This superficial contamination can be overcome using a method that has become well established in recent years: employing short-separation (<10 mm) channels to explicitly measure haemodynamics in the superficial tissues (see section 3.5.3).

## **3.5 FROM ACQUISITION TO DATA ANALYSIS**

### **3.5.1 COMMON INSTRUMENTATION AND ARRAY DESIGN**

As described above, NIRS and Optical Imaging Systems can be broadly sub-divided into three categories based upon the nature of the measurements they obtain. Continuous-wave (CW) systems are the most common, and measure only optical intensity. Included within the CW category are the spatially-resolved spectroscopy (SRS) and cerebral oximetry systems, which tend to be single or dual channel and include the Hamamatsu NIRO and Somanetics Invos systems. Commonly available multi-channel CW systems (which can be used to perform Diffuse Optical Topography and/or Tomography) include the Hitachi ETG series, the NIRx NIRScount system, the TechEn CW6 system and the UCL Optical Imaging System. Frequency-domain (FD) systems measure both optical intensity and phase difference, and a limited number of FD systems are commercially available, including the multi-channel ISS Imagent system. To date there are no commercially available multi-channel time-domain (TD) NIRS systems.

Most commercially available multi-channel systems are customizable in terms of the layout of sources and detectors. This is essential because of the vast range of potential experiments that one may wish to perform. The layout of the array of sources and detectors on the scalp has a huge impact on the quality of NIRS measurements. As such, array design requires careful thought and there are many factors that must be considered. Some of these factors are listed below, but when designing an array it is useful to keep in mind the following: If one were to add together all the PMDFs for all the channels in an ideal array, the resulting 3D distribution would be homogeneous throughout the volume of the brain you wish to study. Designing an array is a process of getting as close as possible to this ideal within the technical limitations of your experiment.

1. Source-detector separation: There is an inherent relationship between source-detector separation and depth sensitivity. The pro-

## Optical Imaging

---

portion of the detected photons that will have travelled through brain tissue increases as source-detector separation increases. However, if the source-detector separation is too great, not enough light will reach the detector to obtain a reliable measurement. Though it depends on the dynamic range of the system, the most commonly selected separation for adult studies is 30 mm, which is long enough to be sensitive to brain tissue but short enough to maintain adequate signal. If the goal is to perform Diffuse Optical Tomography, it is also essential that the array include a range of source-detector separations, each of which will exhibit a different depth sensitivity profile. If possible, the inclusion of short-separation channels ( $\sim 10$  mm or below) can also be extremely beneficial, as they allow superficial signal contamination to be minimized (see section 3.5.3).

2. Channel density: It is clearly beneficial to arrange an array so as to maximise the number of viable channels per unit scalp area. Increasing the number of channels that are sensitive to the volume of interest will increase redundancy, making your experiment more robust to experimental problems, including poor optical contact to the scalp.
3. Channel overlap: Closely related to channel density, when the goal is to perform image reconstruction it is vital that measurement channels are mutually informative. A change in haemoglobin concentration in a given location within the volume of interest should be observable by multiple channels within the array. This is equivalent to saying that the PMDFs of the channels within an array should overlap.
4. Array coverage: Maximising channel density and channel overlap alone will lead to an array with the optical fibres packed as close as possible to one another at the expense of array coverage. It is important that an array covers a sufficiently large area to allow for errors in the placement of the array on the scalp of the subject. Stud-

ies suggest that this error is likely to be of the order of 1 cm [Jurcak et al., 2007].

5. Subject comfort: Ensuring the comfort of the subject is not just an ethical requirement but is also very likely to affect the quality of the resulting data because discomfort will promote motion. Arrays of optical fibres can be heavy, and this can limit the number of possible channels, particularly in studies of infants and children.

Software tools are now emerging to help users of NIRS technologies create and test array designs. Foremost amongst these is the AtlasViewer package of HOMER2 [Aasted et al., 2015]. Users can create and position an array on a virtual head atlas, which allows the areas of the cortex to which the array will be sensitive to be identified.

#### **3.5.2 PARADIGM**

The haemodynamic response (HRF) to functional stimulation, as described in section 3.4.2, can take a few seconds after the start of stimulus presentation to reach its peak and 12-15 seconds after the end of stimulus presentation to return to baseline; its time-course is, however, stimulus-dependent (see Fig. 3.5.1a). The amplitude of the HR is usually much smaller than that of physiological and measurement noise, meaning multiple repetitions of a stimulus are required.

Experimental paradigms that aim to recover the HRF using optical methods can be broadly grouped into two. Event-related designs use many repetitions of a single, short stimulation, separated in time by some inter-stimulus interval. This type of paradigm is mainly used in adult studies [Cutini et al., 2012, Plichta et al., 2006, Hoshi et al., 2011]. Event-related paradigms require many (often  $> 40$ ) trials for each stimulus type because the amplitude of the HR is correlated with the duration of the stimulus, and is therefore small in most event-related designs.

When a train of stimuli are presented, with each train separated by some inter-stimulus interval, the haemodynamic response will have a

## Optical Imaging

---

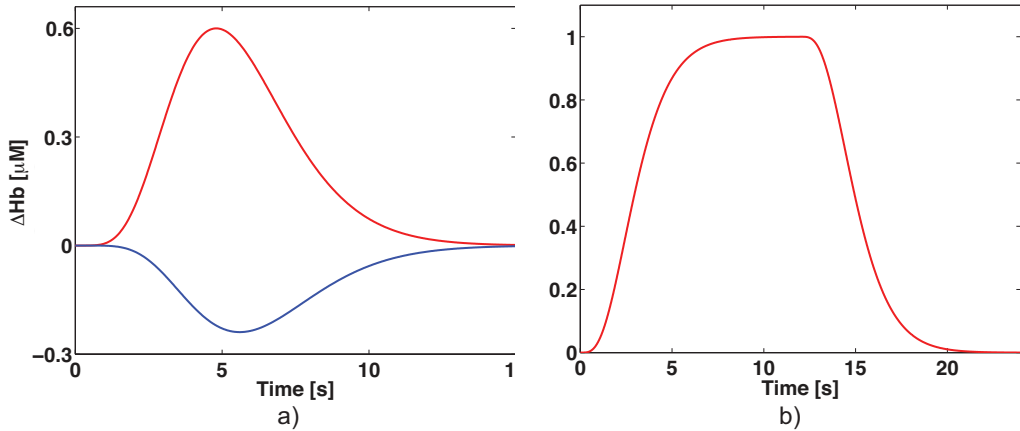


**Figure 3.5.1: Haemodynamic response.** Examples of simulated haemodynamic response function for a) an event-related paradigm (single event presentation) and b) block-designed paradigm (12 seconds of stimulation). Note the different shape of the HRF in the two figures and how it reaches a plateau in the latter.

higher amplitude, a different temporal pattern and a longer duration: the HRF will typically increase after stimulus presentation until it reaches a plateau, where it remains approximately constant until the end of the stimulation block, after which it will return slowly to baseline (see Fig. 3.5.1b). These paradigms, which aim to recover the brain response to a train of stimuli, are referred to as block-design. Block designs are very common in the optics field, primarily because they elicit HRFs with a higher amplitude than event-related paradigms and fewer trials are required to recover the HRF. Block-design paradigms are therefore particularly suitable for infants and challenging populations, since the experiment need only last a few minutes [Ehlis et al., 2007, Lloyd-Fox et al., 2010, Wilcox et al., 2009]. A typical experiment will consist of between 5 and 15 blocks of stimulation, with each block lasting between 5-20 seconds.

Whether an event-related or block design paradigm is applied, the choice of the number of trials and the inter-stimulus interval should be carefully considered. Generally, a higher number of trials will result in a higher signal-to-noise of the recovered HRF. However, a balance must be struck between obtaining a robust estimation of the haemodynamic

### **3.5 From acquisition to data analysis**

---

response and minimizing the duration of the experiment and avoiding the effects of habituation to the stimulus.

When selecting the inter-stimulus interval, the relatively slow response time of the cerebral vasculature must be considered. Depending on the amplitude of the response, an inter-stimulus interval of less than 15 seconds may result in the haemodynamic responses to consecutive stimuli overlapping. This is problematic when a traditional block-averaging method is employed, but a short inter-stimulus interval can be acceptable if the HRF is extracted from the dataset using a deconvolution or general-linear model (GLM) approach (see section 3.5.3 below). When short inter-stimulus intervals are used, the paradigm is referred to as 'fast event-related'. Whether the paradigm is a block, event-related or fast event-related design, jittering the inter-stimulus interval is highly recommended. Altering the duration of the inter-stimulus interval by several seconds in a pseudo-random fashion will minimize the likelihood that oscillatory physiological fluctuations (due to, for example, respiration) will become synchronized with the stimulus paradigm.

In the majority of fNIRS studies, the inter-stimulus period is used as a control condition; haemodynamics that occur during the stimulus period are compared to those that occur during the inter-stimulus interval. During this interval, a subject will typically be requested to remain still and silent, and perhaps fixate on a blank screen. In block-design paradigms, it is also common for a train of different stimuli to be used as a control condition. One example would be for a subject to articulate the months of the year as a control condition for a semantic verbal fluency task. The control condition should be carefully chosen to complement the primary stimulus and minimize the chance of false positives due to blood pressure or motion-related confounds.

#### **3.5.3 DATA ANALYSIS**

The aim of fNIRS data analyses is to recover the haemodynamic response and, in the case of DOT, localize the spatial pattern of that response.

## Optical Imaging

---

Many software toolboxes have been released for optical data analysis and will be described at the end of this section. However, all of these packages are based on the same general processing pipeline (Fig. 3.5.2).

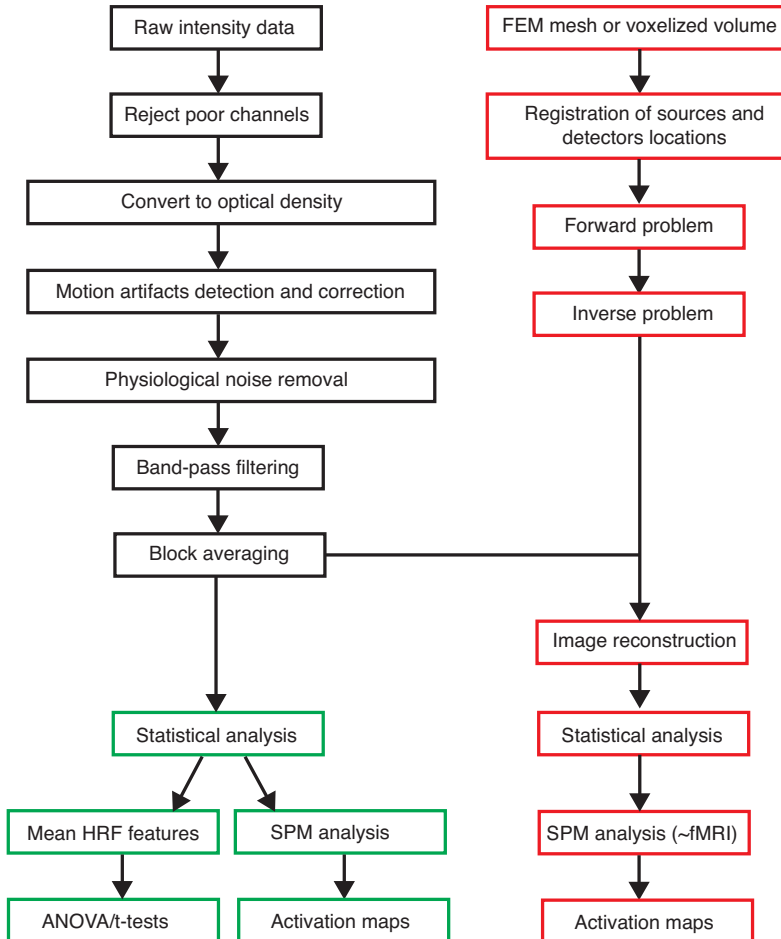


**Figure 3.5.2: Processing pipeline.** General pipeline for fNIRS and DOT data analysis: signal processing steps (black boxes), image reconstruction steps (red boxes) and statistical analysis steps (green boxes).

The majority of CW optical systems measure the raw optical intensity data at two wavelengths for each channel. The baseline intensity value and standard deviation of the intensity are related to amount of light collected by the detector. Channels with very low optical intensity and/or very high standard deviation, are likely to be dominated by instrument noise, and should therefore be removed from the analysis. This will usu-

ally occur because either the source-detector separation is too large, or because of the presence of hair between the optical fibre and the scalp.

Changes in optical intensity at two or more wavelengths can be converted to changes in concentration of HbO and HbR using the MBLL (see section 3.4).

In addition to the haemodynamic response, the typical optical signal is composed of measurement noise, motion artifacts and many forms of physiological noise. Measurement noise can be easily reduced through filtering, but motion and physiological confounds are more difficult to deal with and can easily mask the haemodynamic response. A number of approaches have been developed to reduce these spurious components and recover the actual brain signal.

Optical methods are relatively tolerant of motion; while the optical signal can be transiently impaired by movement of the optical fibre relative to the scalp, data acquired before and after the moment of motion will usually be unaffected. Motion artifacts can be high amplitude, high frequency spikes that are easily detectable in the measured signal (see Fig. 3.5.3), or they can be more subtle, low frequency and low amplitude oscillations, and can even be synchronized with the haemodynamic responses. Their presence can therefore cause false positive detections and it is essential that motion artifacts are removed or at least reduced. The simplest approach is to reject any trial that is contaminated by motion artifacts. However, in some experiments, particularly in challenging populations (e.g. epileptic patients, or infants), very few trials can be recorded, making the rejection process impracticable. An alternative is to use additional devices (e.g. accelerometers) to provide an independent measure of motion artifacts and use regression methods to remove their effect on the optical data [Cui et al., 2015, Virtanen et al., 2011]. The last option, and the most general solution, is to use post-processing techniques that rely on inherent changes in the amplitude and frequency content of the signal to detect and remove motion artifacts. Examples include Principal Component Analysis (PCA) [Zhang et al., 2005, Yücel et al., 2014], Kalman filtering [Izzetoglu et al., 2010], Wavelet filtering [Molavi and Dumont,

## Optical Imaging

---

2012, Chiarelli et al., 2015], correlation-based signal improvement (CBSI) [Cui et al., 2010] and spline interpolation [Scholkmann et al., 2010]. The performance of each technique will depend on the type of motion artifacts; comparison studies have shown that spline interpolation performs very well when motion artifacts can be clearly identified in the measured signal, while Wavelet filtering outperforms other techniques when motion artifacts are more subtle [Brigadoi et al., 2014b, Cooper et al., 2012b].

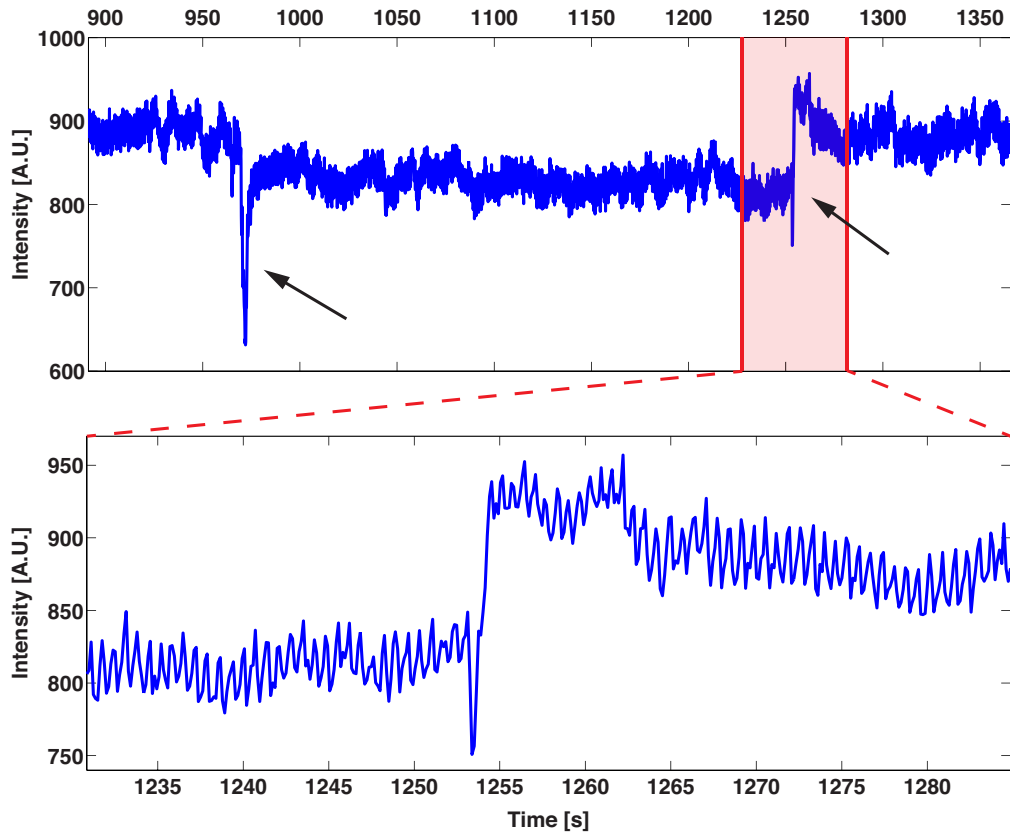


**Figure 3.5.3: Motion artifacts.** Example of spike-like motion artifacts in an optical signal. This type of artifact is easily detectable in the measured signal. Artifacts are identified by black arrows. A magnified version of one of the artifacts is presented at the bottom of the figure.

Physiological noise includes any change in the measured fNIRS signal that has a physiological origin that is not related to the targeted neural activity. Examples of these fluctuations are cardiac activity, respiration,

vasomotor waves (a.k.a. Mayer's waves) and very low frequency oscillations (Fig. 3.5.4). Vasomotor waves are particularly challenging because of the similarity between their frequency content and that of the haemodynamic response. Physiological interference originates from both the cerebral compartment and from the extra-cerebral layers. Skin and skull tissues and the pial layer are highly vascularized. As light travels from the source to the detector, it must pass through these superficial layers twice. As a result, optical measurements are significantly more sensitive to these layers than they are to the brain [Saager and Berger, 2008]. To complicate the situation further, the superficial signal contribution can be time-locked with the stimulus presentation: heart rate and blood pressure increases are common in response to a functional task [Kirilina et al., 2012, Tachtsidis et al., 2009]. These superficial changes can even demonstrate spatial variation across the scalp, and are often mistaken for functional activation of the brain. It is therefore extremely important to minimize physiological noise in order to estimate true brain activity.

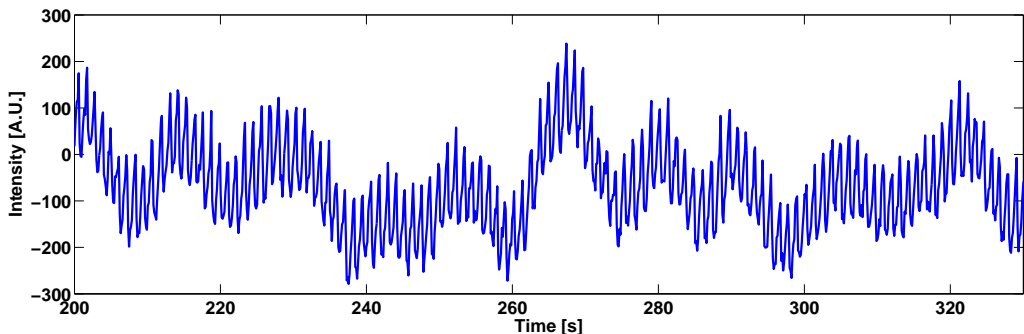


**Figure 3.5.4: Physiological noise.** Example of physiological noise fluctuations in the measured optical signal: heart beat, respiration and vasomotor waves are apparent in this measured signal.

Many studies rely on the assumption that these physiological oscillations are temporally uncorrelated with the functional brain response, and that physiological oscillations are a global effect while the brain response is spatially localized to a small number of measured channels. These assumptions would allow block averaging or PCA techniques to be used to

## Optical Imaging

---

reduce physiological confounds and extract the functional brain response [Lloyd-Fox et al., 2010, Zhang et al., 2005]. However, these assumptions are often unjustified.

Many studies have used additional measurements systems (e.g. pulse oximetry, blood pressure monitoring, fMRI) to explicitly measure physiological oscillations and then regress them from the fNIRS signals [Kirilina et al., 2012, Tachtsidis et al., 2010]. However, additional measurements are not always available and can add to the complexity of an experiment.

One solution to the problem of superficial contamination has been very successful in recent years: the use of so-called short-separation (SS) channels, which have a small source-detector distance (<10 mm). Given the relationship between source-detector distance and depth sensitivity, SS channels are almost exclusively sensitive to the extra-cerebral layers [Saager and Berger, 2005]. The signal measured by SS channels can therefore be regressed from the signal measured by standard separation channels to minimize the effect of physiological noise. Several algorithms have been proposed to perform this regression, including least squares fitting [Saager and Berger, 2008, Gregg et al., 2010], Kalman filtering [Gagnon et al., 2011], adaptive filtering [Zhang et al., 2009], GLM-based analyses [Barker et al., 2013] and Bayesian filtering [Scarpa et al., 2013]. Some of these algorithms perform two-stage processes, where the haemodynamic response is estimated as a final step via block averaging or GLM-approaches, whilst others perform physiological noise reduction and brain response estimation in one step. Since the use of SS channels is a relatively recent advance, regression algorithms are still in development and as yet there is no gold standard method.

Fast event-related designs require different approaches to estimate the haemodynamic response. The short inter-stimulus interval causes consecutive HRFs to overlap substantially. In this situation, the use of block averaging to estimate the haemodynamic response is insufficient. Under the assumption of linearity, deconvolution approaches can, instead, be applied to estimate the underlying HRF. These consist of GLM-based analyses or model-free approaches, where the HRFs to each stimulus

### **3.5 From acquisition to data analysis**

---

type are separated and estimated through deconvolution. It is worth noting that models for the fNIRS haemodynamic response tend to be more complex than the canonical HRF model used in fMRI (see chapter ??), to try to recover more information than size and location of brain activity (e.g., the latency of the activation peak or the temporal profile features). This is permitted partly because of the high temporal resolution of optical devices. The proposed fNIRS HRF models can be divided into two categories: more constrained models (e.g., gamma functions), in which the temporal profile of the HRF has a predefined shape and less constrained models (e.g., set of Gaussian functions), which have been designed to approach a model-free methodology.

If a significant number of channels, with a range of source-detector separations and overlapping sensitivity profiles are obtained, image reconstruction of the recovered HRF can be performed, as described in section 3.4. Another possibility, even if less commonly applied, is to reconstruct the entire acquired data series and then recover the HRF in the image space.

In resting state functional connectivity studies, the aim is to produce spatial maps of regions of the brain which exhibit temporally correlated, low-frequency spontaneous brain activity. The effect of motion artifact on these correlations is difficult to predict, and as a result motion-contaminated data segments are usually rejected before the data is band-pass filtered between 0.009 and 0.08 Hz. Physiological noise regression is also important in these studies, to avoid unwanted physiological correlations being mistaken for functional connectivity [Ferradal et al., 2015, White et al., 2009].

A number of open source software packages are available for optical signal analysis and image reconstruction. The list below is not exhaustive, but includes a range of the most common toolboxes [Scholkmann et al., 2014]:

- HOMER2 (<http://homer-fnirs.org>) [Huppert et al., 2009]: The most popular and widespread software package for fNIRS data analy-

## Optical Imaging

---

sis, HOMER2 is a Matlab-based set of scripts with a user-friendly interface that can be used to filter optical signals and estimate the average haemodynamic response. A number of the motion artifact correction and physiological noise reduction techniques described above have been implemented in HOMER2. AtlasViewer, a package that can produce cortical sensitivity maps of a given array configuration, has recently been added to HOMER2 and should help users to optimize probe design and placement, and improve the inter-subject comparison of optical data [Aasted et al., 2015].

- NIRS-SPM (<http://bispl.weebly.com/nirs-spm.html>) [Ye et al., 2009, Li et al., 2012]: A Matlab-based fNIRS analysis package, NIRS-SPM is founded upon the Statistical Parametric Mapping (SPM) package developed for fMRI [Penny et al., 2011]. NIRS-SPM can produce statistical maps of brain activation overlaid on a brain template that provides some spatial localization, without requiring full image reconstruction approaches.
- NAP (NIRS Analysis Package) [Fekete et al., 2011]: it is a Matlab-based toolbox for fNIRS data analysis, noise reduction and statistical inference. It is based on the GLM.
- POTATO (Platform for Optical Topography Analysis Tools) ([http://www.hitachi-hightech.com/global/products/ind\\_solutions/ict/human/brain/ot/analysis/platform.html](http://www.hitachi-hightech.com/global/products/ind_solutions/ict/human/brain/ot/analysis/platform.html)): Another Matlab-based platform for fNIRS data analysis, POTATO has been developed by Hitachi. It consists of a user-friendly interface and can output 2D topographical activation maps.
- TOAST++ (<http://web4.cs.ucl.ac.uk/research/vis/toast/>) [Schweiger and Arridge, 2014]: Based on C++ but with Matlab and Python interfaces, TOAST++ is a software suite for DOT image reconstruction. It uses an FEM forward solver to simulate the propagation of light in highly scattering media and provides a module with several inverse problem solvers and regularization methods to reconstruct

the spatial distribution of absorption and scattering coefficients.

- NIRFAST (<http://www.dartmouth.edu/nir/nirfast/>) [Dehghani et al., 2009]: A Matlab-based FEM package with a user-friendly interface, NIRFAST can be used to solve the forward and inverse problem in DOT.
- MCX (Monte Carlo Extreme) and MMC (Mesh-based Monte Carlo) (<http://mcx.sourceforge.net/>) [Fang and Boas, 2009, Fang, 2010]: These Monte Carlo simulation packages simulate light propagation in highly scattering media using stochastic modelling methods and can be used to solve the forward problem of DOT. Monte Carlo simulations are thought to provide a more accurate solution to the forward problem compared with FEM-based approaches, particularly in low-scattering media like the cerebrospinal fluid. While MMC requires a finite-element mesh, MCX uses Graphics Processing Units (GPU) to accelerate the computation.
- NAVI (<http://www.nirx.net/software/navi-nirs-tomography-software-by-nirx>): this DOT analysis software has been developed by NIRx. It provides signal processing tools, FEM-based image reconstruction and SPM-like GLM analysis.

#### 3.5.4 STATISTICAL ANALYSIS

Some of the optical analysis software presented above provide statistical analysis tools, while others output only the averaged HRFs or reconstructed images.

The most common statistical approach to optical data analysis is Statistical Parametric Mapping (SPM), which is based on the concept of a GLM [Penny et al., 2011]. The outputs of these methods are activation maps (usually showing t- or z-statistics or p-values), which are corrected for multiple comparisons. If SPM is applied to channel-wise optical data, the resulting activation maps will be created via a process of interpolation and then overlaid on a brain template. In this case, SPM method-

## Optical Imaging

---

ology must be adjusted because stationary Gaussian random field theory cannot be applied to sparse measurement arrays [Tak and Ye, 2014]. However, if the array has sufficient density to allow image reconstruction, SPM can be applied to the image-space data in a manner completely analogous to fMRI.

Other standard statistical methods include Analysis of Variance (ANOVA) and t-tests. Usually some features of the average hemodynamic response are extracted for each subject and channel, e.g. the peak value, the latency of the peak, the area under the curve or the mean value of the HRF in a predefined temporal window around the expected peak. ANOVAs and (paired) t-tests are then performed to statistically infer whether there are significant differences between populations, or between different tasks or channels. It is important to correct the statistical results for multiple comparisons, above all when multi-channel fNIRS or DOT is used.

When resting state functional connectivity analysis is performed, correlation values can be computed, for example with seed-based approaches, where the Pearson correlation coefficient is computed between a chosen time series and all other signals. Another approach is to use Independent Component Analysis (ICA) to derive independent individual components. Either way, correlation values or ICA components can be directly compared with t-tests or transformed to z scores by Fisher's z transform and statistically analysed with ANOVAs or t-tests.

For a detailed description of the statistical analysis of fNIRS data see [Tak and Ye \[2014\]](#).

### 3.6 EXAMPLES OF APPLICATION

In this section, we describe some exemplar applications of optical techniques. The first example reports important results obtained in fNIRS studies of infants [[Lloyd-Fox et al., 2012](#), [Homae et al., 2010](#)]. The study of brain function and neurocognitive development in infants is a field in which optical methods have begun to reach their significant potential.

### **3.6 Examples of application**

---

The second example describes the use of optical methods in the neonatal clinic to study seizures [Singh et al., 2014]. The last example illustrates the state-of-the-art of DOT methods. High-density DOT is applied to study both healthy and pathological adults. This work highlights the tremendous progress optical techniques have achieved in recent years [Eggebrecht et al., 2014].

#### **3.6.1 FUNCTIONAL STUDIES OF THE INFANT BRAIN**

The processing of the human voice in the infant brain is an important topic of research in cognitive neuroscience. The ability to process human voice is fundamental to social interaction. Studies have shown that humans develop the ability to distinguish voices from non-vocal sounds very early in life, even prenatally. It is extremely important to localize and understand the regions of the brain in which voice processing occurs, and at what age infants start to show voice-specific cortical function. This information is important from a neurodevelopment perspective, but is also crucial to the study of disorders such as autism and schizophrenia, which cause impaired social cognition.

Lloyd-Fox et al. [2012] used fNIRS to investigate this topic. While fMRI studies of voice processing in infants have been reported, the technique requires the infant subjects to be asleep. fNIRS studies can be performed on awake infants, in more suitable environments. Lloyd-Fox et al. [2012] presented thirty-three healthy 4 to 7 month-old infants with non-speech voice sounds and familiar non-voice sounds and studied the brain specialization to the two stimuli, as well as its development of the responses with age. Examples of non-speech voice sounds include laughing, crying, yawning and coughing, while examples of non-voice sounds include running water and the rattling of toys. In order to keep infants' attention, visual stimuli were presented in synchrony with the auditory stimuli. To account for the potential impact of this visual stimulus, a third condition was presented: visual stimulation only. Haemodynamic responses to the visual-only condition were subtracted from the responses of the two au-

## Optical Imaging

---

ditory conditions, to take into account the impact of the visual presentation. The paradigm consisted of a 10 s baseline trial (consisting of static images of transport) followed by a 10 s of stimulation (which could be one of the three conditions) in a pseudo random order. A minimum of four valid trials per condition was required to include the infant in the final analysis. A 38-channel fNIRS array was placed bilaterally over the inferior frontal cortex and both the anterior and posterior portions of the superior temporal regions (aST and pST respectively).

The results of this study showed a localized bilateral activation over the aST in response to the voice stimuli, but a more widespread bilateral activation over the inferior frontal region and both the aST and pST in response to non-voice stimuli. In particular, the aST showed a greater haemodynamic response to the voice condition compared to the non-voice condition. It is hypothesised that the greater activation to non-voice stimuli in the pST could reflect an immature response, since these results are not replicated in adults. [Lloyd-Fox et al. \[2012\]](#) performed a correlation analysis to evaluate the relationship between the age of the participant and the amplitude of the response to stimuli. This analysis revealed a significant correlation between the two only in the voice condition. These results provide evidence that cerebral specialization in response to human voice sounds emerges during the first 6 months of life and that infants are able to discriminate between voice and non-voice stimuli at this early age.

Another interesting application of optical techniques in infants is the study of global functional networks. It is well known that these networks play an important role in human cognition and behaviour, and that the infant brain rapidly develops both short- and long-range connectivity. The investigation of how and when these global networks emerge in early infancy is important because they may be an important biomarker for healthy cognitive development. From a structural brain development perspective, there are two contrasting hypotheses on the development of functional connectivity between cortical areas. The first is that there is an increase in functional connectivity with age, due to the increase in

### 3.6 Examples of application

myelination over the postnatal period. The second hypothesis is that a decrease should be observed because of the number of synaptic connections is known to decrease shortly after birth.

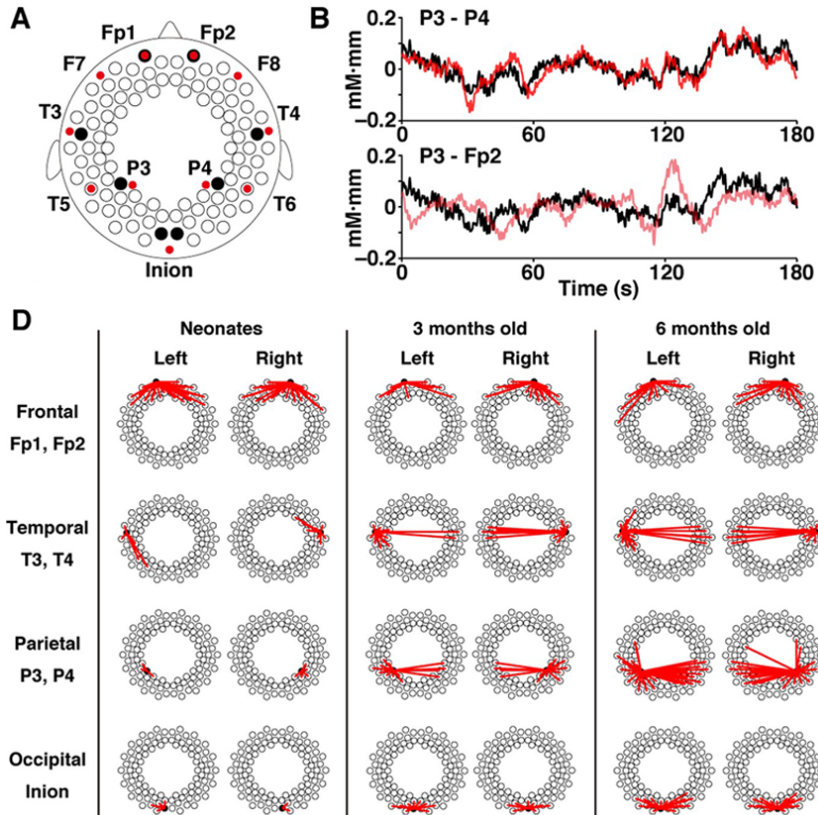


**Figure 3.6.1: Infant functional networks.** Adapted with permission from [Homae et al., 2010]. A) The 94-channel fNIRS array located over the frontal, parietal, temporal and occipital areas. B) Examples of data before the filtering procedure for two channels with high temporal correlation and two channels with low temporal correlation. D) Significant correlations between areas for all ages.

Homae et al. [2010] used fNIRS to investigate this critical question. Fifty-two healthy full-term infants, of which 15 were neonates, 21 were 3-months old and 16 were 6-months old, were investigated in this study. A 94-channel fNIRS array was located over the frontal, parietal, temporal and occipital areas as shown in Fig. 3.6.1A. The resulting signals were band-pass filtered (cut-off frequencies at 0.009 and 0.08 Hz), and 3 minutes of good quality, motion-free data was extracted for further anal-

## Optical Imaging

---

ysis. The Pearson's correlation coefficient was computed between the time course of each channel and all other channels (see Fig. 3.6.1D). In Fig. 3.6.1B, examples of data before the filtering procedure are shown for two channels with high temporal correlation and two channels with low temporal correlation. As can be seen from Fig. 3.6.1D, long-range correlations appear to develop with age. In neonates, high correlations are found between multiple channels in the frontal region, both within and between hemispheres, but only very weak correlations were observed with other brain areas. The inter-hemispheric correlations across the frontal regions were maintained (but somewhat reduced) in the 3-month and 6-month old infants, while inter-hemispheric correlations develop between many other regions, particularly the temporal, parietal and occipital cortices. The authors performed a further cluster analysis to spatially identify regions with similar temporal correlations. These results suggest that functional networks start to become bilaterally organized during the first 3 months of life and might be related to the functional maturation of the corpus callosum. Another interesting result of this study was that correlations increased with age only in channels located in the left parietal and temporal regions, but not in their homologous right-hemisphere channels. This left-lateralization in the development of functional connectivity might be associated with the leftward structural asymmetry of the arcuate fasciculus in adults. Finally, the authors demonstrated that there is a particular spatial pattern of functional correlations (localized over the left hemisphere, across the frontal and occipital areas) that shows a decrease in connectivity between term and 3-months of age, but an increase in connectivity between 3 and 6 months of age. The authors hypothesized that this pattern might be evidence of a reorganization of the connections between frontal and posterior areas at different developmental stages. Functional networks were therefore found to exhibit spatially specific, age-related growth and decline over the first few months of life.

#### **3.6.2 NEONATAL CLINICAL APPLICATION**

Seizures are a common symptom of neonatal brain injury, but are also independently associated with a poor clinical outcome. Neonatal seizures are thought to be significantly under diagnosed, are poorly classified and are difficult to treat. Electroencephalography (EEG, see chapter ?? for more information on the EEG technique) is commonly applied in the study of seizures and epileptic conditions, but continuous EEG monitoring is not standard clinical practice. This is at least in part due to the fact that interpreting neonatal EEG is very challenging, and there is a complex and unpredictable relationship between clinical symptoms of seizure and neonatal EEG. Furthermore, seizures are a spatially varying phenomenon, which can be related to the underlying brain pathology and the spatial resolution of EEG is severely limited. For these reasons, the application of DOT in the study of infant seizure has significant promise.

In 2014, [Singh et al. \[2014\]](#) were able to produce the first ever DOT images of a seizure in the new-born infant. This required the integration of DOT and EEG. The EEG trace was used simply as a marker for seizure events, which allowed the haemodynamic impact of the EEG-identified seizures to be investigated. [Singh et al. \[2014\]](#) used the 16 paired-source, 16 detector UCL Optical Imaging System and a flexible head cap (Fig. 3.6.2) to record 58 individual DOT channels positioned across the scalp. Thirteen EEG electrodes were also embedded into the flexible cap to allow EEG to be acquired in the clinical neonatal EEG montage. The head cap allowed simultaneous DOT and EEG recording to take place for an extended period without risking the comfort of the infant.

In this case-study, [Singh et al. \[2014\]](#) performed simultaneous DOT and EEG on an infant who had suffered a hypoxic ischaemic insult shortly after being born at term age. The infant then underwent a period of clinical hypothermia, during which its body temperature was reduced by several degrees in an effort to minimise neurological injury. [Singh et al. \[2014\]](#) were able to identify 7 seizures in a 60 minute DOT-EEG recording

## Optical Imaging

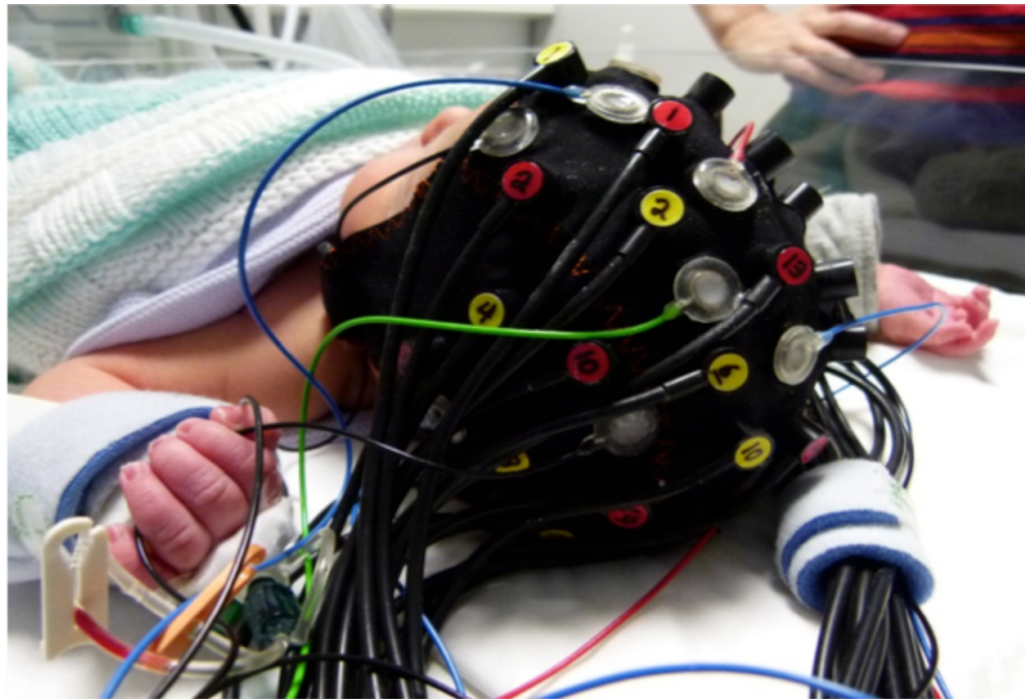


**Figure 3.6.2: Example of cap.** The flexible head cap used to accommodate both optodes and electrodes is displayed on the baby's head. (Taken with permission from [Singh et al., 2014]).

during the period where the infant's body temperature was returned to normal. These seizures were independently identified from the EEG data by two neurophysiologists.

The first major result of this paper was that the observed haemodynamic response to the seizure events was extremely large. In fact, it was clearly visible in the unprocessed DOT signals. When analysed using a typical, channel-wise NIRS approach, the peak seizure-induced change in HbO was found to be  $12.4 \mu\text{M}$ . This should be compared to a typical adult functional response, which is usually on the order of  $1 \mu\text{M}$  [Lloyd-Fox et al., 2010, Gagnon et al., 2014, Huppert et al., 2006]. The scale of these changes is important, because if the haemodynamic response to a seizure is large enough to be observed without averaging, it provides evidence that continuous DOT monitoring may improve seizure detection.

The morphology of the seizure-induced changes in HbO and HbR iden-

### 3.6 Examples of application

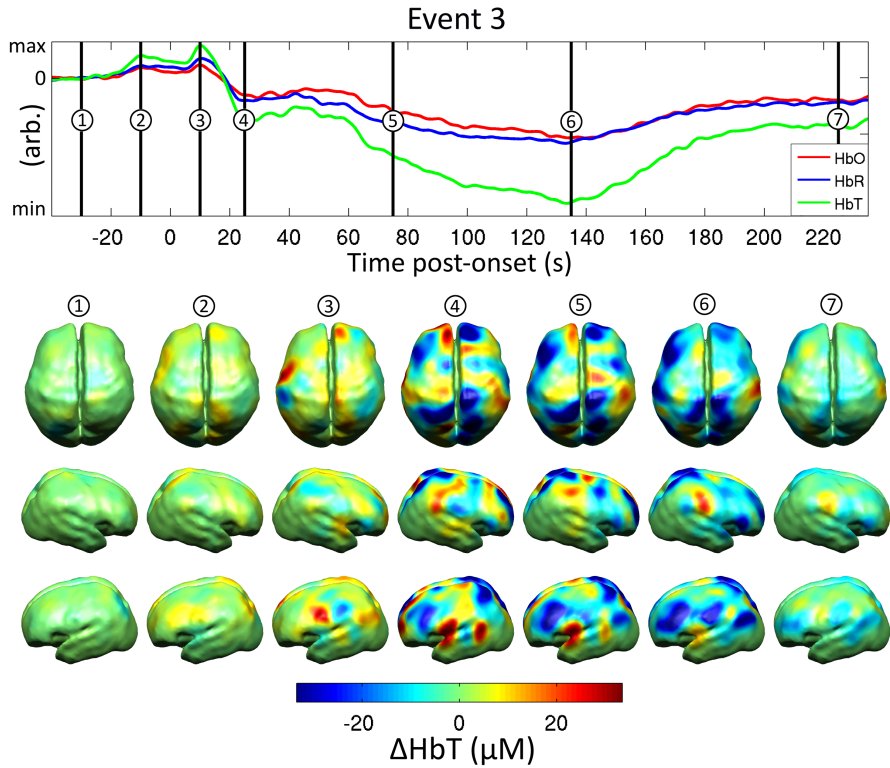


**Figure 3.6.3: Example of a seizure event.** A biphasic response is apparent in the DOT data with an increase in blood volume, followed by a prolonged decrease in blood volume, which last several minutes. HbO (in red), HbR (in blue) and HbT (in green) are displayed and represent the average of the concentration changes during one of the seizure events (event 3) across all channels. A sequence of reconstructed images showing 7 particular time points of the changes in HbT are displayed at the bottom of the figure. Dorsal and left and right lateral views are shown. (Taken with permission from [Singh et al., 2014]).

tified in this infant were also significant. The seven identified seizures exhibited a highly consistent pattern of haemodynamic changes. This consisted of an initial increase in HbO and HbR, followed by a sudden and prolonged decrease in HbO and HbR relative to the pre-seizure state. This period of decreased blood volume was found to last several minutes in some cases. Fig. 3.6.3a summarizes this biphasic morphology. Fig. 3.6.3b also exhibits an example of an imaging sequence that was obtained through linear reconstruction of the DOT data using a bespoke, spatially-registered and age matched neonatal atlas [Brigadói et al., 2014a]. Inter-

## Optical Imaging

---

estingly, the spatial distribution of seizure-induced changes in HbO, HbR and HbT (total haemoglobin, sum of HbO and HbR) was also found to be extremely consistent between seizure events.

While the authors admit that a single case study is not sufficient to draw any clinical or physiological conclusions, this investigation provides an exciting demonstration of the utility of DOT imaging in the clinical environment.

### 3.6.3 HEALTHY AND PATHOLOGICAL ADULTS

DOT technology has advanced dramatically in recent years, with high-density approaches achieving increased spatial resolution and anatomical localization and improvements in signal processing allowing greater sensitivity and specificity. Despite these advances, certain challenges have hindered the acceptance of DOT as a standard neuroimaging technique. First, DOT imaging systems tend to have a severely limited field of view (i.e. are only able to cover a limited brain area). This is because of the challenge of building an instrument and patient interface with a sufficiently high number of channels. Second, DOT acquisitions suffer from superficial tissue contamination (as discussed above) and third, DOT obtains no structural information about the brain, and accurate image reconstruction and interpretation requires DOT measurements to be spatially registered to a structural image (be it a subject-specific MRI or atlas).

In their seminal paper, [Eggebrecht et al. \[2014\]](#) demonstrate that all these fundamental limitations can now be overcome. They present a high-density DOT system that is able to map distributed brain function and resting state networks in both healthy and pathological adults. Their results demonstrate that high-density DOT is now a robust alternative to more traditional functional neuroimaging techniques. [Eggebrecht et al. \[2014\]](#) describe a system consisting of 96 sources and 92 detectors, which together provide more than 1200 channels at varying source-detector distances, the shortest being 13 mm. This configuration provides high sensi-

### **3.6 Examples of application**

---

tivity to regions up to 10 mm below the pial surface while also allowing the effects of superficial haemodynamics to be removed. The authors also demonstrate an imaging array designed to provide maximum comfort to the participant, as well as stable, high-quality optical coupling to scalp.

Advances in MRI segmentation, finite element modelling, registration and photon migration simulations were all exploited to efficiently create subject-specific head models, sensitivity profiles and high-quality reconstructed images.

Eight healthy adults participated in experiments that were designed to highlight the imaging quality that can be obtained by DOT by direct, within-subject comparison with fMRI images. Functional paradigms consisting of visual stimulation with a flickering checkerboard and more subtle auditory and language stimulation were used to test the ability of the system to map distributed brain function. During the language paradigm, subjects were instructed to either listen to, to read, to imagine themselves reading or to produce a verb associated with a presented word. These functional stimulation paradigms demonstrated an exceptional correspondence between DOT and fMRI activation (Fig. 3.6.4). Resting state data were also acquired for a 10-minute period to test the ability of the system to map resting state networks. A seed-based analysis was employed to study the spatial pattern of functional connectivity. Again, fMRI and DOT results were highly consistent, with the dorsal attention network, the fronto-parietal control network and the default mode network showing both intra- and inter-hemispheric functional connectivity via both modalities. To demonstrate the advantages of DOT approaches, three patients with Parkinson's disease and implanted deep-brain stimulation electrodes, who are unable to undergo MRI, performed the language and resting state protocol with DOT. The results of both the functional paradigms and the resting state analysis were similar to those of the healthy group.

Although Eggebrecht et al. [2014] were successful in demonstrating the state-of-the-art of DOT methodology, several limitations are still appar-

## Optical Imaging

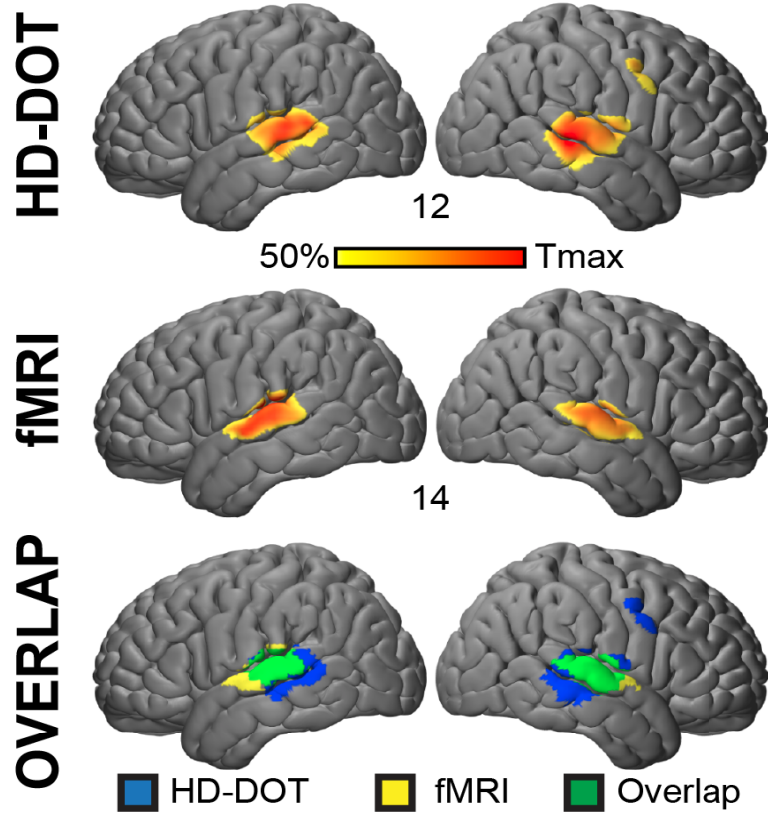


**Figure 3.6.4: Comparison between DOT and fMRI results.** Example of group average results for one language paradigm (listening to speech) for both DOT and fMRI. In the last row, a map of the overlap between the results of the two techniques is displayed. (Taken with permission from [Cooper, 2014]).

ent in their approach. For example, the spatial resolution of their high-density DOT system is still lower than that of fMRI (approximately 13 mm vs. 6 mm) and, like most optical methods, their system has limited depth sensitivity and can only be used to study the cortical surface. Furthermore, the use of subject-specific structural MRI in the image reconstruction procedure (though it minimizes localization errors) negates one of the major advantages of optical techniques. Atlas-based approaches have been proven to be an effective solution [Cooper et al., 2012a] to this problem, but do result in additional error. Despite these concerns, the remarkable advances in high-density DOT achieved by Eggebrecht

## BIBLIOGRAPHY

---

et al. [2014] are likely to mark a watershed moment in the development and uptake of optical imaging methods. The next great technological leap will be to produce high-density optical imaging systems with a truly portable, or even wearable, construction. This technology would allow optical methods to fully reach their potential of allowing functional neuroimaging to take place in almost any environment.

## BIBLIOGRAPHY

- Aasted, C. M., Ycel, M. A., Cooper, R. J., Dubb, J., Tsuzuki, D., Becerra, L., Petkov, M. P., Borsook, D., Dan, I., and Boas, D. A. Anatomical guidance for functional near-infrared spectroscopy: Atlasviewer tutorial. *Neurophotonics*, 2(2):020801, 2015. doi: 10.1117/1.NPh.2.2.020801. URL <http://dx.doi.org/10.1117/1.NPh.2.2.020801>.
- Arridge, S. R. Optical tomography in medical imaging. *Inverse Problems*, 15(2):R41–R93, 1999.
- Austin, T., Gibson, A., Branco, G., Yusof, R. M., Arridge, S., Meek, J., Wyatt, J., Delpy, D., and Hebden, J. Three dimensional optical imaging of blood volume and oxygenation in the neonatal brain. *Neuroimage*, 31(4):1426–1433, 2006.
- Bandettini, P. A., Wong, E. C., Hinks, R. S., Tikofsky, R. S., and Hyde, J. S. Time course EPI of human brain function during task activation. *Magnetic resonance in medicine : official journal of the Society of Magnetic Resonance in Medicine / Society of Magnetic Resonance in Medicine*, 25(2):390–7, 1992.
- Barker, J. W., Aarabi, A., and Huppert, T. J. Autoregressive model based algorithm for correcting motion and serially correlated errors in fnirs. *Biomedical optics express*, 4(8):1366–1379, 2013.
- Bluestone, A., Abdoulaev, G., Schmitz, C., Barbour, R., and Hielscher,

## Optical Imaging

---

- A. Three-dimensional optical tomography of hemodynamics in the human head. *Optics express*, 9(6):272–286, 2001.
- Boas, D. A., Brooks, D. H., Miller, E. L., DiMarzio, C. A., Kilmer, M., Gaudette, R. J., and Zhang, Q. Imaging the body with diffuse optical tomography. *Signal Processing Magazine, IEEE*, 18(6):57–75, 2001.
- Boas, D. A., Elwell, C. E., Ferrari, M., and Taga, G. Twenty years of functional near-infrared spectroscopy: introduction for the special issue. *NeuroImage*, 85 Pt 1:1–5, 2014.
- Brazy, J. E., Lewis, D. V., Mitnick, M. H., and vander Vliet, F. F. J. Noninvasive monitoring of cerebral oxygenation in preterm infants: preliminary observations. *Pediatrics*, 75(2):217–225, 1985.
- Brigadoi, S., Aljabar, P., Kuklisova-Murgasova, M., Arridge, S. R., and Cooper, R. J. A 4d neonatal head model for diffuse optical imaging of pre-term to term infants. *Neuroimage*, 100:385–394, 2014a.
- Brigadoi, S., Ceccherini, L., Cutini, S., Scarpa, F., Scatturin, P., Selb, J., Gagnon, L., Boas, D. A., and Cooper, R. J. Motion artifacts in functional near-infrared spectroscopy: A comparison of motion correction techniques applied to real cognitive data. *NeuroImage*, 85 Pt 1:181–91, 2014b.
- Chance, B., Zhuang, Z., UnAh, C., Alter, C., and Lipton, L. Cognition-activated low-frequency modulation of light absorption in human brain. *Proceedings of the National Academy of Sciences of the United States of America*, 90(8):3770–4, 1993.
- Chiarelli, A. M., Maclin, E. L., Fabiani, M., and Gratton, G. A kurtosis-based wavelet algorithm for motion artifact correction of fnirs data. *NeuroImage*, 112:128–137, 2015.
- Cooper, R. J. Bioimaging: Watching the brain at work. *Nature Photonics*, 8(6):425–426, 2014.

## BIBLIOGRAPHY

---

- Cooper, R. J., Caffini, M., Dubb, J., Fang, Q., Custo, A., Tsuzuki, D., Fischl, B., Wells, W., Dan, I., and Boas, D. A. Validating atlas-guided dot: a comparison of diffuse optical tomography informed by atlas and subject-specific anatomies. *NeuroImage*, 62(3):1999–2006, 2012a.
- Cooper, R. J., Selb, J., Gagnon, L., Phillip, D., Schytz, H. W., Iversen, H. K., Ashina, M., and Boas, D. A. A systematic comparison of motion artifact correction techniques for functional near-infrared spectroscopy. *Frontiers in neuroscience*, 6:147, 2012b.
- Cope, M. and Delpy, D. T. System for long-term measurement of cerebral blood and tissue oxygenation on newborn infants by near infra-red transillumination. *Medical and Biological Engineering and Computing*, 26 (3):289–294, 1988.
- Cui, X., Bray, S., and Reiss, A. L. Functional near infrared spectroscopy (NIRS) signal improvement based on negative correlation between oxygenated and deoxygenated hemoglobin dynamics. *NeuroImage*, 49 (4):3039–46, 2010.
- Cui, X., Baker, J. M., Liu, N., and Reiss, A. L. Sensitivity of fnirs measurement to head motion: An applied use of smartphones in the lab. *Journal of neuroscience methods*, 245:37–43, 2015.
- Cutini, S., Scarpa, F., Scatturin, P., Dell’Acqua, R., and Zorzi, M. Number-space interactions in the human parietal cortex: Enlightening the snarc effect with functional near-infrared spectroscopy. *Cerebral Cortex*, page bhs321, 2012.
- Dehghani, H., Eames, M. E., Yalavarthy, P. K., Davis, S. C., Srinivasan, S., Carpenter, C. M., Pogue, B. W., and Paulsen, K. D. Near infrared optical tomography using nirfast: Algorithm for numerical model and image reconstruction. *Communications in numerical methods in engineering*, 25 (6):711–732, 2009.

## Optical Imaging

---

- Eggebrecht, A. T., Ferradal, S. L., Robichaux-Viehoever, A., Hassanpour, M. S., Dehghani, H., Snyder, A. Z., Hershey, T., and Culver, J. P. Mapping distributed brain function and networks with diffuse optical tomography. *Nature photonics*, 8(6):448–454, 2014.
- Ehlis, A.-C., Herrmann, M. J., Plichta, M. M., and Fallgatter, A. J. Cortical activation during two verbal fluency tasks in schizophrenic patients and healthy controls as assessed by multi-channel near-infrared spectroscopy. *Psychiatry Research: Neuroimaging*, 156(1):1–13, 2007.
- Enfield, L., Cantanhede, G., Douek, M., Ramalingam, V., Purushotham, A., Hebden, J., and Gibson, A. Monitoring the response to neoadjuvant hormone therapy for locally advanced breast cancer using three-dimensional time-resolved optical mammography. *Journal of biomedical optics*, 18(5):056012–056012, 2013.
- Fang, Q. Mesh-based Monte Carlo method using fast ray-tracing in Plücker coordinates. *Biomedical optics express*, 1(1):165–75, 2010.
- Fang, Q. and Boas, D. A. Monte Carlo simulation of photon migration in 3D turbid media accelerated by graphics processing units. *Optics express*, 17(22):20178–90, 2009.
- Fekete, T., Rubin, D., Carlson, J. M., and Mujica-Parodi, L. R. The nirs analysis package: Noise reduction and statistical inference. *PloS one*, 6(9):e24322, 2011.
- Ferradal, S. L., Eggebrecht, A. T., Hassanpour, M., Snyder, A. Z., and Culver, J. P. Atlas-based head modeling and spatial normalization for high-density diffuse optical tomography: in vivo validation against fmri. *Neuroimage*, 85:117–126, 2014.
- Ferradal, S. L., Liao, S. M., Eggebrecht, A. T., Shimony, J. S., Inder, T. E., Culver, J. P., and Smyser, C. D. Functional imaging of the developing brain at the bedside using diffuse optical tomography. *Cerebral Cortex*, page bhu320, 2015.

## BIBLIOGRAPHY

---

- Ferrari, M., Giannini, I., Sideri, G., and Zanette, E. Continuous non invasive monitoring of human brain by near infrared spectroscopy. In *Oxygen Transport to Tissue VII*, pages 873–882. Springer, 1985.
- Ferrari, M. and Quaresima, V. A brief review on the history of human functional near-infrared spectroscopy (fNIRS) development and fields of application. *NeuroImage*, 63(2):921–35, 2012.
- Fox, P. T. and Raichle, M. E. Focal physiological uncoupling of cerebral blood flow and oxidative metabolism during somatosensory stimulation in human subjects. *Proceedings of the National Academy of Sciences*, 83(4):1140–1144, 1986.
- Gagnon, L., Perdue, K., Greve, D. N., Goldenholz, D., Kaskhedikar, G., and Boas, D. A. Improved recovery of the hemodynamic response in diffuse optical imaging using short optode separations and state-space modeling. *Neuroimage*, 56(3):1362–1371, 2011.
- Gagnon, L., Yücel, M. A., Boas, D. A., and Cooper, R. J. Further improvement in reducing superficial contamination in nirs using double short separation measurements. *Neuroimage*, 85:127–135, 2014.
- Gregg, N. M., White, B. R., Zeff, B. W., Berger, A. J., and Culver, J. P. Brain specificity of diffuse optical imaging: improvements from superficial signal regression and tomography. *Frontiers in neuroenergetics*, 2, 2010.
- Hebden, J. and Delpy, D. Diagnostic imaging with light. *British journal of radiology*, 70(Special-Issue-1):S206–S214, 1997.
- Hebden, J. C., Gibson, A., Yusof, R. M., Everdell, N., Hillman, E. M., Delpy, D. T., Arridge, S. R., Austin, T., Meek, J. H., and Wyatt, J. S. Three-dimensional optical tomography of the premature infant brain. *Physics in medicine and biology*, 47(23):4155, 2002.
- Homae, F., Watanabe, H., Otobe, T., Nakano, T., Go, T., Konishi, Y., and Taga, G. Development of global cortical networks in early infancy. *The Journal of neuroscience*, 30(14):4877–4882, 2010.

## Optical Imaging

---

- Hoshi, Y. and Tamura, M. Detection of dynamic changes in cerebral oxygenation coupled to neuronal function during mental work in man. *Neuroscience letters*, 150(1):5–8, 1993.
- Hoshi, Y., Huang, J., Kohri, S., Iguchi, Y., Naya, M., Okamoto, T., and Ono, S. Recognition of human emotions from cerebral blood flow changes in the frontal region: a study with event-related near-infrared spectroscopy. *Journal of Neuroimaging*, 21(2):e94–e101, 2011.
- Huppert, T. J., Diamond, S. G., Franceschini, M. A., and Boas, D. A. HomER: a review of time-series analysis methods for near-infrared spectroscopy of the brain. *Applied optics*, 48(10):D280–98, 2009.
- Huppert, T., Hoge, R., Diamond, S., Franceschini, M. A., and Boas, D. A. A temporal comparison of bold, asl, and nirs hemodynamic responses to motor stimuli in adult humans. *Neuroimage*, 29(2):368–382, 2006.
- Izzetoglu, M., Chitrapu, P., Bunce, S., and Onaral, B. Motion artifact cancellation in NIR spectroscopy using discrete Kalman filtering. *Biomedical engineering online*, 9:16, 2010.
- Jöbsis, F. F. Noninvasive, infrared monitoring of cerebral and myocardial oxygen sufficiency and circulatory parameters. *Science*, 198(4323):1264–7, 1977.
- Jurcak, V., Tsuzuki, D., and Dan, I. 10/20, 10/10, and 10/5 systems revisited: their validity as relative head-surface-based positioning systems. *Neuroimage*, 34(4):1600–1611, 2007.
- Kato, T., Kamei, A., Takashima, S., and Ozaki, T. Human visual cortical function during photic stimulation monitoring by means of near-infrared spectroscopy. *Journal of cerebral blood flow and metabolism*, 13(3):516–20, 1993.
- Kirilina, E., Jelzow, A., Heine, A., Niessing, M., Wabnitz, H., Brühl, R., Ittermann, B., Jacobs, A. M., and Tachtsidis, I. The physiological ori-

## BIBLIOGRAPHY

---

- gin of task-evoked systemic artefacts in functional near infrared spectroscopy. *NeuroImage*, 61(1):70–81, 2012.
- Kwong, K. K., Belliveau, J. W., Chesler, D. A., Goldberg, I. E., Weisskoff, R. M., Poncelet, B. P., Kennedy, D. N., Hoppel, B. E., Cohen, M. S., and Turner, R. Dynamic magnetic resonance imaging of human brain activity during primary sensory stimulation. *Proceedings of the National Academy of Sciences of the United States of America*, 89(12):5675–9, 1992.
- Li, H., Tak, S., and Ye, J. C. Lipschitz-killing curvature based expected euler characteristics for p-value correction in fnirs. *Journal of neuroscience methods*, 204(1):61–67, 2012.
- Lloyd-Fox, S., Blasi, A., and Elwell, C. Illuminating the developing brain: the past, present and future of functional near infrared spectroscopy. *Neuroscience & Biobehavioral Reviews*, 34(3):269–284, 2010.
- Lloyd-Fox, S., Blasi, A., Mercure, E., Elwell, C., and Johnson, M. H. The emergence of cerebral specialization for the human voice over the first months of life. *Social neuroscience*, 7(3):317–330, 2012.
- Maki, A., Yamashita, Y., Ito, Y., Watanabe, E., Mayanagi, Y., and Koizumi, H. Spatial and temporal analysis of human motor activity using non-invasive nir topography. *Medical physics*, 22(12):1997–2005, 1995.
- Matthes, K. and Gross, F. Fortlaufende registrierung der lichtabsorption des blutes in zwei spektralbezirken. *Arch Exp Pathol Pharmakol*, 191: 831–831, 1939.
- Meek, J. H., Firbank, M., Elwell, C. E., Atkinson, J., Braddick, O., and Wyatt, J. S. Regional hemodynamic responses to visual stimulation in awake infants. *Pediatric Research*, 43(6):840–843, 1998.
- Millikan, G. Experiments on muscle haemoglobin in vivo; the instantaneous measurement of muscle metabolism. *Proceedings of the Royal Society of London. Series B, Biological Sciences*, 123(831):218–241, 1937.

## Optical Imaging

---

- Mintun, M. A., Lundstrom, B. N., Snyder, A. Z., Vlassenko, A. G., Shulman, G. L., and Raichle, M. E. Blood flow and oxygen delivery to human brain during functional activity: theoretical modeling and experimental data. *Proceedings of the National Academy of Sciences*, 98(12): 6859–6864, 2001.
- Molavi, B. and Dumont, G. A. Wavelet-based motion artifact removal for functional near-infrared spectroscopy. *Physiological measurement*, 33(2): 259–70, 2012.
- Ogawa, S., Tank, D. W., Menon, R., Ellermann, J. M., Kim, S. G., Merkle, H., and Ugurbil, K. Intrinsic signal changes accompanying sensory stimulation: functional brain mapping with magnetic resonance imaging. *Proceedings of the National Academy of Sciences of the United States of America*, 89(13):5951–5, 1992.
- Okada, F., Tokumitsu, Y., Hoshi, Y., and Tamura, M. Impaired interhemispheric integration in brain oxygenation and hemodynamics in schizophrenia. *European archives of psychiatry and clinical neuroscience*, 244(1):17–25, 1994.
- Pellicer, A., Greisen, G., Benders, M., Claris, O., Dempsey, E., Fumagalli, M., Gluud, C., Hagmann, C., Hellström-Westas, L., Hyttel-Sorensen, S., et al. The safeboosc phase ii randomised clinical trial: a treatment guideline for targeted near-infrared-derived cerebral tissue oxygenation versus standard treatment in extremely preterm infants. *Neonatology*, 104(3):171–178, 2013.
- Penny, W. D., Friston, K. J., Ashburner, J. T., Kiebel, S. J., and Nichols, T. E. *Statistical parametric mapping: the analysis of functional brain images: the analysis of functional brain images*. Academic press, 2011.
- Piper, S. K., Krueger, A., Koch, S. P., Mehnert, J., Habermehl, C., Steinbrink, J., Obrig, H., and Schmitz, C. H. A wearable multi-channel fnirs system for brain imaging in freely moving subjects. *Neuroimage*, 85: 64–71, 2014.

## BIBLIOGRAPHY

---

- Plichta, M., Herrmann, M., Baehne, C., Ehlis, A.-C., Richter, M., Pauli, P., and Fallgatter, A. Event-related functional near-infrared spectroscopy (fnirs): are the measurements reliable? *Neuroimage*, 31(1):116–124, 2006.
- Saager, R. and Berger, A. Measurement of layer-like hemodynamic trends in scalp and cortex: implications for physiological baseline suppression in functional near-infrared spectroscopy. *Journal of biomedical optics*, 13 (3):034017, 2008.
- Saager, R. B. and Berger, A. J. Direct characterization and removal of interfering absorption trends in two-layer turbid media. *Journal of the Optical Society of America A*, 22(9):1874, 2005.
- Sasai, S., Homae, F., Watanabe, H., Sasaki, A. T., Tanabe, H. C., Sadato, N., and Taga, G. A nirs-fmri study of resting state network. *Neuroimage*, 63(1):179–193, 2012.
- Scarpa, F., Brigadói, S., Cutini, S., Scatturin, P., Zorzi, M., Dell’acqua, R., and Sparacino, G. A reference-channel based methodology to improve estimation of event-related hemodynamic response from fNIRS measurements. *NeuroImage*, 72:106–19, 2013.
- Scholkmann, F., Spichtig, S., Muehlemann, T., and Wolf, M. How to detect and reduce movement artifacts in near-infrared imaging using moving standard deviation and spline interpolation. *Physiological measurement*, 31(5):649–62, 2010.
- Scholkmann, F., Kleiser, S., Metz, A. J., Zimmermann, R., Mata Pavia, J., Wolf, U., and Wolf, M. A review on continuous wave functional near-infrared spectroscopy and imaging instrumentation and methodology. *NeuroImage*, 85 Pt 1:6–27, 2014.
- Schweiger, M. and Arridge, S. The toast++ software suite for forward and inverse modeling in optical tomography. *Journal of biomedical optics*, 19 (4):040801–040801, 2014.

## Optical Imaging

---

- Severinghaus, J. W. and Honda, Y. History of blood gas analysis. vii. pulse oximetry. *Journal of clinical monitoring*, 3(2):135–138, 1987.
- Singh, H., Cooper, R. J., Lee, C. W., Dempsey, L., Edwards, A., Brigadói, S., Airantzis, D., Everdell, N., Michell, A., Holder, D., et al. Mapping cortical haemodynamics during neonatal seizures using diffuse optical tomography: A case study. *NeuroImage: Clinical*, 5:256–265, 2014.
- Steinbrink, J., Villringer, A., Kempf, F., Haux, D., Boden, S., and Obrig, H. Illuminating the bold signal: combined fmri–fnirs studies. *Magnetic resonance imaging*, 24(4):495–505, 2006.
- Suzuki, S., Takasaki, S., Ozaki, T., and Kobayashi, Y. Tissue oxygenation monitor using nir spatially resolved spectroscopy. In *BiOS'99 International Biomedical Optics Symposium*, pages 582–592. International Society for Optics and Photonics, 1999.
- Tachtsidis, I., Leung, T. S., Chopra, A., Koh, P. H., Reid, C. B., and Elwell, C. E. False positives in functional near-infrared topography. *Advances in experimental medicine and biology*, 645:307–14, 2009.
- Tachtsidis, I., Koh, P. H., Stubbs, C., and Elwell, C. E. Functional optical topography analysis using statistical parametric mapping (spm) methodology with and without physiological confounds. In *Oxygen Transport to Tissue XXXI*, pages 237–243. Springer, 2010.
- Tak, S. and Ye, J. C. Statistical analysis of fnirs data: a comprehensive review. *NeuroImage*, 85:72–91, 2014.
- Villringer, A., Planck, J., Hock, C., Schleinkofer, L., and Dirnagl, U. Near infrared spectroscopy (NIRS): a new tool to study hemodynamic changes during activation of brain function in human adults. *Neuroscience letters*, 154(1-2):101–4, 1993.
- Virtanen, J., Noponen, T., Kotilahti, K., Virtanen, J., and Ilmoniemi, R. J. Accelerometer-based method for correcting signal baseline changes

## BIBLIOGRAPHY

---

- caused by motion artifacts in medical near-infrared spectroscopy. *Journal of biomedical optics*, 16(8):087005, 2011.
- Watanabe, E., Yamashita, Y., Maki, A., Ito, Y., Koizumi, H., and Mayanagi, Y. Infrared spectroscopy as noninvasive functional mapping of human brain. *Neuroscience Research Supplements*, 19:S267, 1994.
- White, B. R., Snyder, A. Z., Cohen, A. L., Petersen, S. E., Raichle, M. E., Schlaggar, B. L., and Culver, J. P. Resting-state functional connectivity in the human brain revealed with diffuse optical tomography. *Neuroimage*, 47(1):148–156, 2009.
- Wilcox, T., Bortfeld, H., Woods, R., Wruck, E., Armstrong, J., and Boas, D. Hemodynamic changes in the infant cortex during the processing of featural and spatiotemporal information. *Neuropsychologia*, 47(3):657–662, 2009.
- Wyatt, J., Delpy, D., Cope, M., Wray, S., and Reynolds, E. Quantification of cerebral oxygenation and haemodynamics in sick newborn infants by near infrared spectrophotometry. *The Lancet*, 328(8515):1063–1066, 1986.
- Ye, J. C., Tak, S., Jang, K. E., Jung, J., and Jang, J. Nirs-spm: statistical parametric mapping for near-infrared spectroscopy. *Neuroimage*, 44(2):428–447, 2009.
- Yücel, M. A., Selb, J., Cooper, R. J., and Boas, D. A. Targeted principle component analysis: A new motion artifact correction approach for near-infrared spectroscopy. *Journal of innovative optical health sciences*, 7 (02), 2014.
- Zeff, B. W., White, B. R., Dehghani, H., Schlaggar, B. L., and Culver, J. P. Retinotopic mapping of adult human visual cortex with high-density diffuse optical tomography. *Proceedings of the National Academy of Sciences*, 104(29):12169–12174, 2007.

## Optical Imaging

---

Zhang, Q., Strangman, G. E., and Ganis, G. Adaptive filtering to reduce global interference in non-invasive nirs measures of brain activation: how well and when does it work? *Neuroimage*, 45(3):788–794, 2009.

Zhang, Y., Brooks, D. H., Franceschini, M. A., and Boas, D. A. Eigenvector-based spatial filtering for reduction of physiological interference in diffuse optical imaging. *Journal of biomedical optics*, 10(1):11014, 2005.